



Bifurcation and pattern formation driven by implicit memory and nonlocal perception in diffusive resource-consumer systems

Luhong Ye ^{a,b,*}, Hao Wang ^b

^a School of Mathematics and Physics, Anqing Normal University, 246133, Anqing, PR China

^b Department of Mathematical and Statistical Sciences, University of Alberta, T6G 2G1, Edmonton, AB, Canada

ARTICLE INFO

Keywords:

Implicit memory
Nonlocal perception
Cognitive diffusion
Top-hat function
Turing bifurcation
Hopf bifurcation
Turing-Hopf bifurcation

ABSTRACT

Understanding how animals perceive and remember their environments is essential for modeling ecological population dynamics. In this study, we investigate two diffusive resource-consumer systems that incorporate implicit spatial memory and nonlocal perception, key cognitive traits observed in higher animals. The models employ a biologically motivated top-hat kernel to describe finite-range perception and introduce memory as a dynamic variable governed by biologically plausible mechanisms. We develop a coupled PDE-ODE nonlinear framework that captures these cognitive processes and derive conditions for Turing, Hopf, and Turing-Hopf bifurcations. Unlike classical reaction-diffusion systems, our approach reveals richer spatiotemporal behaviors resulting from the interplay between memory and perception. Analytical results are supported by numerical simulations that show the emergence of complex patterns, including oscillating stripes, spots, and mixed structures. Our findings demonstrate how cognitive traits like memory decay and nonlocal sensing affect population distribution and stability, leading to outcomes such as spatial heterogeneity, periodic cycles, or extinction. This work contributes to a deeper understanding of animal movement ecology and offers theoretical tools for predicting population responses to environmental changes.

1. Introduction

Spatial cognition significantly influences population movements, encompassing three primary cognitive components: perception, memory, and learning. Therefore, incorporating these cognition-based processes into animal movement models is essential. Recently, an increasing number of researchers have considered spatial memory in population models and examined its impacts on population dynamics, particularly in highly developed animals (e.g., [1–17]). Typically, diffusion is employed to model the spatial movements of organisms. However, the traditional diffusion equation, derived from energy conservation and Fick's law, has limitations when directly applied to population movements, especially since highly developed animals often move based on memory. For instance, [1] demonstrated that certain animals exhibiting memory-based behaviors also perform regular spatial movements. Additionally, [3] indicated that blue whales utilize chlorophyll distributions for their migratory paths. However, memory effects tend to diminish over time, necessitating the inclusion of delays in models. Normally, delays are introduced into the response term, representing processes such as population maturation or incubation. However, delays induced by spatial memory appear specifically within the diffusion term, as demonstrated in [7,9–16]. Most research to date has concentrated on explicit memory, wherein foragers directly reference past experiences. Nevertheless, implicit memory, a type that does not explicitly reference prior experiences [1,6], represents a distinct

* Corresponding author.

E-mail address: leaf07@163.com (L. Ye).

<https://doi.org/10.1016/j.cnsns.2025.109593>

Received 1 June 2025; Received in revised form 7 November 2025; Accepted 9 December 2025

Available online 11 December 2025

1007-5704/© 2025 Elsevier B.V. All rights are reserved, including those for text and data mining, AI training, and similar technologies.

and higher-level brain function involving the storage of perceived information. Research on implicit memory remains sparse, and most existing studies assume populations diffuse within localized ranges.

In many scenarios, perceptual ability is assumed to rely purely on local information. Since Fagan et al. [2] proposed a resource-consumer system modeling the interplay between perceptual ranges and foraging success, local perception and learning mechanisms have attracted considerable research attention [6,17–19]. Wang et al. [6] introduced a resource-consumer model incorporating a term that biases consumer movement, accounting for non-uniform perceptual abilities over varying distances (an instance of nonlocal perception). They suggested that animals implicitly remember to follow or avoid areas of high population density. Subsequently, Shi et al. [17] proposed two systems incorporating a local perceptual function $q(x, t)$, which explicitly represents implicit memory derived from consumer learning and memory fading:

$$\begin{cases} u_t = d_1 \Delta u + u(1 - u/k) - \frac{mu v}{u+1}, (x, t) \in \Omega \times (0, +\infty), \\ v_t = d_2 \Delta v - \chi \nabla \cdot (v \nabla q) + \frac{mu v}{u+1} - d v, (x, t) \in \Omega \times (0, +\infty), \\ q_t = bu - \gamma q, (x, t) \in \Omega \times (0, +\infty), \\ \partial_\nu u = \partial_\nu v = 0, x \in \partial\Omega, t > 0, \end{cases}$$

and

$$\begin{cases} u_t = d_1 \Delta u + u(1 - u/k) - \frac{mu v}{u+1}, (x, t) \in \Omega \times (0, +\infty), \\ v_t = d_2 \Delta v - \chi \nabla \cdot (v \nabla q) + \frac{mu v}{u+1} - d v, (x, t) \in \Omega \times (0, +\infty), \\ q_t = bu v - (\gamma + \xi v) q, (x, t) \in \Omega \times (0, +\infty), \\ \partial_\nu u = \partial_\nu v = 0, x \in \partial\Omega, t > 0. \end{cases}$$

Here, $u(x, t)$, $v(x, t)$ represent densities of resource and consumer populations. Shi et al. analyzed the spectra of the linearized operators and investigated the conditions for Hopf and Turing bifurcations. In these models, implicit memory is explicitly described by an additional equation. The first scenario models population movement responding to landscape markers (such as urine, feces, or footprints) left by other populations, with marks accumulating linearly relative to resource availability and decaying constantly. The term bu indicates attraction to resource-rich areas. The second scenario differs in that implicit memory resides within the foragers' cognition. Individuals recall locations of recent encounters with members of other populations and adapt their movements accordingly. Additionally, it assumes intra-population communication, allowing individuals to share collective expectations about other populations' distributions. Here, buv captures consumer-resource encounters, while ξ signifies the cognitive decay rate caused by repeated visits to the same location and conflicting sensory inputs.

However, [17] considered only the effect of local perception, wherein the perceptual range is very narrow. In most cases, perceptual ability relies solely on local information, implying that interactions occur only among individuals occupying the same spatial location—these are termed local behaviors. In reality, perception should not be restricted in this manner, as nonlocal cues such as visual and auditory signals also significantly inform animal movements. The concept of nonlocal interactions in single-species population systems was first proposed by Furter et al. [18], who introduced an integral form involving a kernel function. Subsequently, several researchers [20–26] have extensively investigated how nonlocal perception influences population dynamics. Typically, nonlocal terms in these studies represent spatial averages, suggesting that the growth rate at a specific location is influenced by the average population density across the entire spatial domain. Wang et al. [6] utilized a top-hat kernel function to model nonlocal perception:

$$K_R(z) = \begin{cases} \frac{1}{2R}, & |z| \leq R, \\ 0, & \text{otherwise,} \end{cases}$$

where $R \geq 0$ denotes the nonlocal perception radius. This implies that a population perceives resources within a fixed distance R from its current location, whereas resources beyond this radius remain undetected, thus nullifying the perception ability. For example, when wildebeest could track the availability of their resources at the 100 km scale, but there was no migration when the foragers based their movement decision on purely local information by [2]. However, the Gaussian and exponential detection functions in [20–26], respectively, allow the agent to perceive nearby resources most clearly and decays monotonically as the distance from the observation location increases. Consequently, the top-hat kernel function offers a more realistic representation, as animals typically possess restricted habitats but broad perceptual ranges. The influence of the top-hat kernel function on population dynamics has been extensively studied in [17,26,27].

Table 1
Parameter descriptions.

Parameter	Description
d_1	The Fickian diffusion coefficient of the resource
d_2	The Fickian diffusion coefficient of the consumer
d_3	The cognitive diffusion rate
β	The carrying capacity
R	The perceptual scale
m	The encounter rate between resources and consumers
s	The consumer's intrinsic growth rate
b	The growth rate
γ	The decay rate due to finite memory capacity
ξ	The decay rate associated with consumers returning to areas with low resource density
\mathbf{n}	The normal vector on $\partial\Omega$

Motivated by the preceding analysis, we formulate two diffusive resource-consumer systems that incorporate implicit memory and nonlocal perception, subject to Neumann boundary conditions:

$$\begin{cases} \frac{\partial u}{\partial t} = d_1 \Delta u + u(1 - \beta u) - \frac{mu v}{u + 1}, (x, t) \in \Omega \times (0, +\infty), \\ \frac{\partial v}{\partial t} = d_2 \Delta v - d_3 \nabla \cdot (v \nabla q) + s v (1 - \frac{v}{u}), (x, t) \in \Omega \times (0, +\infty), \\ q_t = b \hat{u} - \gamma q, (x, t) \in \Omega \times (0, +\infty), \\ \frac{\partial u}{\partial \mathbf{n}} = \frac{\partial v}{\partial \mathbf{n}} = 0, x \in \partial\Omega, t > 0, \end{cases} \quad (1.1)$$

and

$$\begin{cases} \frac{\partial u}{\partial t} = d_1 \Delta u + u(1 - \beta u) - \frac{mu v}{u + 1}, (x, t) \in \Omega \times (0, +\infty), \\ \frac{\partial v}{\partial t} = d_2 \Delta v - d_3 \nabla \cdot (v \nabla q) + s v (1 - \frac{v}{u}), (x, t) \in \Omega \times (0, +\infty), \\ q_t = b \hat{u} v - (\gamma + \xi v) q, (x, t) \in \Omega \times (0, +\infty), \\ \frac{\partial u}{\partial \mathbf{n}} = \frac{\partial v}{\partial \mathbf{n}} = 0, x \in \partial\Omega, t > 0, \end{cases} \quad (1.2)$$

where

$$\hat{u} = \int_{\Omega} K_R(x - y) u(y, t) dy,$$

and the kernel function K_R is the top-hat function. Systems (1.1)–(1.2) indicate that consumers can perceive nonlocal resource densities and recall locations where resources were previously encountered. Additionally, implicit memory is treated as a dynamically evolving quantity that continuously updates as consumers traverse their habitats, allowing memories to form and reshape over time. Here $b\hat{u}$ indicates attraction to resource-rich areas by nonlocal perception. $b\hat{u}v$ means consumer-resource encounters as the consumers rely on the memory for the distribution of the resources in certain areas. Clearly, systems (1.1)–(1.2) differ significantly from classical reaction-diffusion systems, presenting additional analytical challenges for investigating their dynamics.

Descriptions of all parameters are provided in Table 1. All parameters are positive constants except for $d_3 \in \mathbb{R}$, where specifically, $d_3 > 0$ (or < 0) indicates attraction toward regions of higher (or lower) population density. We assume that the two populations inhabit the isolated and bounded region $\Omega = (0, l\pi)$, with $l \in \mathbb{R}^+$ and a smooth boundary $\partial\Omega$. The imposed boundary condition reflects that the populations exist within a closed environment to describe animal movement better by [6] and [17].

In the following sections, we primarily investigate the dynamics of systems (1.1)–(1.2) to identify additional dynamical properties and to explore how implicit memory and nonlocal perception influence the spatiotemporal distributions of populations. Since pattern formation is essential for understanding species distributions, our analysis provides theoretical insights into the mechanisms underlying spatial population dynamics. The remainder of this paper is organized as follows: Section 2 examines the dynamics of systems (1.1)–(1.2) without nonlocal interactions; Section 3 investigates the dynamics of systems (1.1)–(1.2) with nonlocal interactions, including numerical simulations to support theoretical findings. Finally, Section 4 concludes the paper with a concise summary of the main results.

2. Dynamics without nonlocal perception

In this section, we investigate conditions of the stability and bifurcations for systems (1.1)–(1.2) in the absence of nonlocality, which are

$$\begin{cases} \frac{\partial u}{\partial t} = d_1 \Delta u + u(1 - \beta u) - \frac{mu v}{u+1}, (x, t) \in \Omega \times (0, +\infty), \\ \frac{\partial v}{\partial t} = d_2 \Delta v - d_3 \nabla \cdot (v \nabla q) + sv(1 - \frac{v}{u}), (x, t) \in \Omega \times (0, +\infty), \\ q_t = bu - \gamma q, (x, t) \in \Omega \times (0, +\infty), \\ \frac{\partial u}{\partial \mathbf{n}} = \frac{\partial v}{\partial \mathbf{n}} = 0, x \in \partial\Omega, t > 0, \end{cases} \quad (2.1)$$

and

$$\begin{cases} \frac{\partial u}{\partial t} = d_1 \Delta u + u(1 - \beta u) - \frac{mu v}{u+1}, (x, t) \in \Omega \times (0, +\infty), \\ \frac{\partial v}{\partial t} = d_2 \Delta v - d_3 \nabla \cdot (v \nabla q) + sv(1 - \frac{v}{u}), (x, t) \in \Omega \times (0, +\infty), \\ q_t = buv - (\gamma + \xi v)q, (x, t) \in \Omega \times (0, +\infty), \\ \frac{\partial u}{\partial \mathbf{n}} = \frac{\partial v}{\partial \mathbf{n}} = 0, x \in \partial\Omega, t > 0. \end{cases} \quad (2.2)$$

2.1. Dynamics of (2.1)

In this subsection, we verify the conditions of stability and bifurcations of (2.1), and validate theoretical results by simulations. Through direct calculations, system (2.1) has a unique constant equilibrium $E^* = (u^*, v^*, q^*) = (\alpha, \alpha, b\alpha/\gamma)$, where

$$\alpha = \frac{1 - m - \beta + \sqrt{(1 - m - \beta)^2 + 4\beta}}{2\beta}.$$

Linearizing system (2.1) at E^* gives

$$\frac{\partial}{\partial t} \begin{pmatrix} u \\ v \\ q \end{pmatrix} = D_1 \Delta \begin{pmatrix} u \\ v \\ q \end{pmatrix} + A \begin{pmatrix} u \\ v \\ q \end{pmatrix},$$

where

$$D_1 = \begin{pmatrix} d_1 & 0 & 0 \\ 0 & d_2 & -d_3\alpha \\ 0 & 0 & 0 \end{pmatrix}, \quad A = \begin{pmatrix} 1 - \beta\alpha - \frac{m\alpha}{(\alpha+1)^2} & -\frac{m\alpha}{\alpha+1} & 0 \\ s & s-2 & 0 \\ b & 0 & -\gamma \end{pmatrix}.$$

Hence, we obtain the characteristic equation

$$|\lambda I_3 + D_1 \mu_n - A| = 0, \quad n \in \mathbb{N}, \quad (2.3)$$

where $\mu_n = (n/l)^2$, $n \in \mathbb{N}_0$, and I_3 is the unit matrix. (2.3) simplifies to

$$\lambda^3 + A_n \lambda^2 + B_n \lambda + C_n = 0,$$

where

$$A_n = (d_1 + d_2)\mu_n + \beta\alpha + \frac{m\alpha}{(\alpha+1)^2} + 1 - s + \gamma = [d_1\mu_n - 1 + \beta\alpha + \frac{m\alpha}{(\alpha+1)^2}] + [d_2\mu_n - s + 2] + \gamma,$$

$$B_n = [(d_1 + d_2)\mu_n + \beta\alpha + \frac{m\alpha}{(\alpha+1)^2} + 1 - s]\gamma + [d_1\mu_n - 1 + \beta\alpha + \frac{m\alpha}{(\alpha+1)^2}][d_2\mu_n - s + 2] + \frac{sm\alpha}{\alpha+1},$$

$$C_n = \gamma[d_1\mu_n - 1 + \beta\alpha + \frac{m\alpha}{(\alpha+1)^2}][d_2\mu_n - s + 2] + \frac{d_3 b m \alpha^2}{\alpha+1} \mu_n + \frac{\gamma s m \alpha}{\alpha+1}.$$

For $n = 0$, (2.3) reduces to

$$(\lambda + \gamma) \left\{ \lambda^2 - \left[s - 1 - \alpha\beta - \frac{m\alpha}{(\alpha+1)^2} \right] \lambda + \left[1 - \alpha\beta - \frac{m\alpha}{(\alpha+1)^2} \right] (s - 2) + \frac{sm\alpha}{\alpha+1} \right\} = 0.$$

If

$$\begin{cases} s - 1 - \alpha\beta - \frac{m\alpha}{(\alpha+1)^2} = [1 - \alpha\beta - \frac{m\alpha}{(\alpha+1)^2}] + (s - 2) < 0, \\ [1 - \alpha\beta - \frac{m\alpha}{(\alpha+1)^2}](s - 2) + \frac{sm\alpha}{\alpha+1} > 0, \end{cases} \quad (2.4)$$

then E^* is locally asymptotically stable for the non-spatial system of (2.1).

In order to analyse the spectral, we denote

$$X = W_N^{2,p}(\Omega) \times W_N^{2,p}(\Omega) \times W^{2,p}(\Omega), \quad Y = L^p(\Omega) \times L^p(\Omega) \times W_N^{2,p}(\Omega),$$

where

$$W_N^{2,p}(\Omega) = \{u \in W^{2,p}(\Omega) : \partial_n u = 0 \text{ on } \partial\Omega\}.$$

From the previous linearization, we obtain the linear operator

$$\mathfrak{L} \begin{pmatrix} \phi \\ \psi \\ \varphi \end{pmatrix} = \begin{pmatrix} d_1 \Delta \phi + (1 - \beta\alpha - \frac{m\alpha}{(\alpha+1)^2})\phi - \frac{m\alpha}{\alpha+1}\psi \\ d_2 \Delta \psi - d_3 \alpha \Delta \varphi + s\phi + (s-2)\psi \\ b\phi - \gamma\varphi \end{pmatrix}, \quad (2.5)$$

here linear operator \mathfrak{L} is closed with $D(X) = \mathfrak{L}$, showing that $\phi \in W_N^{2,p}(\Omega)$, $\psi \in W_N^{2,p}(\Omega)$, and $\varphi \in W^{2,p}(\Omega)$. From [28], the following conclusions are obtained.

Theorem 2.1. *Spectrum of \mathfrak{L} is*

$$\sigma(\mathfrak{L}) = \sigma_p(\mathfrak{L}) = S \cup \{-\gamma\},$$

here

$$S = \{\mu_n^{(1)}\}_{n=0}^{+\infty} \cup \{\mu_n^{(2)}\}_{n=0}^{+\infty} \cup \{\mu_n^{(3)}\}_{n=0}^{+\infty}, \quad (2.6)$$

and $\mu_n^{(j)}$ ($j = 1, 2, 3$) are the characteristic roots satisfying $\Re(\mu_n^{(1)}) < \Re(\mu_n^{(2)}) < \Re(\mu_n^{(3)})$.

Proof. Consider the following nonhomogeneous problem

$$\begin{cases} d_1 \Delta \phi + (1 - \beta\alpha - \frac{m\alpha}{(\alpha+1)^2})\phi - \frac{m\alpha}{\alpha+1}\psi = \mu\phi + \tau_1, \\ d_2 \Delta \psi - d_3 \alpha \Delta \varphi + s\phi + (s-2)\psi = \mu\psi + \tau_2, \\ b\phi - \gamma\varphi = \mu\varphi + \tau_3, \\ \partial_n \phi = \partial_n \psi = 0, \end{cases} \quad (2.7)$$

here $\mu \in \mathbb{C}$ and $(\tau_1, \tau_2, \tau_3) \in Y$.

Firstly, consider the case $\mu + \gamma \neq 0$, then (2.7) can be simplified to

$$\begin{cases} d_1 \Delta \phi + (1 - \beta\alpha - \frac{m\alpha}{(\alpha+1)^2})\phi - \frac{m\alpha}{\alpha+1}\psi = \mu\phi + \tau_1, \\ d_2 \Delta \psi - \frac{d_3 \alpha}{\mu + \gamma}(b\Delta \varphi - \Delta \tau_3) + s\phi + (s-2)\psi = \mu\psi + \tau_2, \\ \partial_n \phi = \partial_n \psi = 0, \end{cases}$$

that is

$$\mathfrak{L}_1 \begin{pmatrix} \phi \\ \psi \end{pmatrix} = \begin{pmatrix} d_1 \Delta \phi + (1 - \beta\alpha - \frac{m\alpha}{(\alpha+1)^2})\phi - \frac{m\alpha}{\alpha+1}\psi - \mu\phi \\ d_2 \Delta \psi - \frac{d_3 \alpha}{\mu + \gamma}b\Delta \varphi + s\phi + (s-2)\psi - \mu\psi \end{pmatrix} = \begin{pmatrix} \tau_1 \\ \tau_2 - \frac{d_3 \alpha}{\mu + \gamma}\Delta \tau_3 \end{pmatrix}. \quad (2.8)$$

As $\phi, \psi \in W_N^{2,p}(\Omega)$ and set

$$\phi = \sum_{n=0}^{+\infty} a_n \phi_n, \quad \psi = \sum_{n=0}^{+\infty} b_n \phi_n. \quad (2.9)$$

From (2.8) and (2.9), integrate (2.8) and obtain

$$\begin{pmatrix} -d_1 \mu_n + (1 - \beta\alpha - \frac{m\alpha}{(\alpha+1)^2}) - \mu & -\frac{m\alpha}{\alpha+1} \\ \frac{d_3 \alpha b}{\mu + \gamma} \mu_n + s & -d_2 \mu_n + s - 2 - \mu \end{pmatrix} \begin{pmatrix} a_n \\ b_n \end{pmatrix} = \begin{pmatrix} \int_0^{l\pi} \tau_1 dx \\ \int_0^{l\pi} (\tau_2 - \frac{d_3 \alpha}{\mu + \gamma} \Delta \tau_3) dx \end{pmatrix}.$$

With $\tau_1 = \tau_2 = \tau_3 = 0$, then $\text{Ker}(\mathfrak{L}_1) = \{(0, 0)^T\}$ and $\text{Ker}(\mathfrak{L} - \mu I)$ is $\{(0, 0, 0)^T\}$. As it is injective, then get

$$\begin{vmatrix} -d_1 \mu_n + (1 - \beta\alpha - \frac{m\alpha}{(\alpha+1)^2}) - \mu & -\frac{m\alpha}{\alpha+1} \\ \frac{d_3 \alpha b}{\mu + \gamma} \mu_n + s & -d_2 \mu_n + s - 2 - \mu \end{vmatrix} \neq 0,$$

that is

$$\left(\mu + d_1 \mu_n - (1 - \beta\alpha - \frac{m\alpha}{(\alpha+1)^2}) \right) (\mu + 2 - s + d_2 \mu_n) + \frac{m\alpha}{\alpha+1} \left(\frac{d_3 \alpha b}{\mu + \gamma} \mu_n + s \right) \neq 0. \quad (2.10)$$

(2.5) implies that $\mathfrak{L} - \mu I$ is surjective. According to [29], it is also bijective. Furthermore, $(\mathfrak{L} - \mu I)^{-1}$ is bounded and

$$\|\phi\|_{W_N^{2,p}(\Omega)} + \|\psi\|_{W_N^{2,p}(\psi)} \leq \|(\mathfrak{L} - \mu I)^{-1}\| \left(\|d_1 \Delta \phi + 1 - \beta\alpha - \frac{m\alpha}{(\alpha+1)^2} \phi - \frac{m\alpha}{\alpha+1} \psi\|_{L^p(\Omega)} + \|d_2 \Delta \psi - \frac{d_3 \alpha b}{\mu + \gamma} \Delta \phi + s\phi + (s-2)\psi\|_{L^p(\Omega)} \right).$$

Hence, μ lies in resolvent set of \mathfrak{L} and does not belong to spectrum set if (2.10) is satisfied. Otherwise, then the characteristic equation owns roots $\mu_n^{(j)}$ ($j = 1, 2, 3$) for each $n \in \mathbb{N}_0$. Set $\tau_j = 0$ ($j = 1, 2, 3$), and take $\mu_n^{(j)}$ in (2.7). Therefore, obtain

$$\begin{pmatrix} \phi \\ \psi \\ \varphi \end{pmatrix} = \begin{pmatrix} \phi^{(j)} \\ \psi^{(j)} \\ \varphi^{(j)} \end{pmatrix} = \begin{pmatrix} 1 \\ \frac{\alpha+1}{m\alpha} [-d_1 \mu_n - \mu_n^{(j)} + \frac{m\alpha}{(\alpha+1)^2} + \alpha\beta - 1] \\ \frac{b}{\gamma + \mu_n^{(j)}} \end{pmatrix} \phi_n,$$

which means that $\text{Ker}(\mathfrak{L} - \mu_n^{(j)}) = \text{Span}\{(\phi^{(j)}, \psi^{(j)}, \varphi^{(j)})^T\}$. Thus, eigenvalues of \mathfrak{L} are $\mu_n^{(j)}$ ($j = 1, 2, 3$), and $\mu_n^{(j)} \in \sigma_p(\mathfrak{L})$.

Secondly, consider the case $\mu + \gamma = 0$. (2.7) can be turned into

$$\begin{cases} \psi = \frac{\alpha+1}{bm\alpha} [d_1 \Delta \tau_3 + (1 - \beta\alpha - \frac{m\alpha}{(\alpha+1)^2}) \tau_3 + \gamma \tau_3 - b\tau_1], \\ \Delta \varphi = \frac{1}{\alpha d_3} [d_2 \Delta \psi - \frac{s\tau_3}{b} + (s-2+\gamma)\psi - \tau_2]. \end{cases}$$

Let $\tau_i = 0$ ($i = 1, 2, 3$), then obtain $\text{Ker}(\mathfrak{L} + \gamma I) = \text{Span}\{(0, 0, \tilde{\varphi})^T\}$ as $\Delta \tilde{\varphi} = 0$ and $-\gamma \in \sigma_p(\mathfrak{L})$. This ends the proof. \square

From Theorem 2.1, we have the following result.

Theorem 2.2. *The equilibrium E^* of system (2.1) is locally stable if all roots of the characteristic equation own negative real parts; otherwise, it is unstable.*

Next, we discuss bifurcation conditions for (2.1). E^* is stable if and only if

$$A_n > 0; \quad C_n > 0; \quad A_n B_n - C_n > 0.$$

Otherwise, system (2.1) undergoes bifurcations. The specific bifurcation conditions for various cases are discussed below, choosing the cognitive diffusion d_3 as the bifurcation parameter.

From $C_n = 0$, we get

$$d_3^*(\gamma) = -\frac{\alpha+1}{bm\alpha^2\mu_n} \left\{ \frac{\gamma sm\alpha}{\alpha+1} + [d_1 \mu_n - 1 + \beta\alpha + \frac{m\alpha}{(\alpha+1)^2}] [d_2 \mu_n - s + 2] \gamma \right\}. \quad (2.11)$$

By $A_n B_n - C_n = 0$, we obtain

$$d_3^{**}(\gamma) = \frac{\alpha+1}{bm\alpha^2\mu_n} \left\{ A_n B_n - \frac{\gamma sm\alpha}{\alpha+1} - \gamma [d_1 \mu_n - 1 + \beta\alpha + \frac{m\alpha}{(\alpha+1)^2}] [d_2 \mu_n - s + 2] \right\}. \quad (2.12)$$

By (2.4), $B_n > 0$ holds. (2.11) ((2.12)) indicates that the consumers can attract toward regions of lower (higher) population density, then system (2.1) undergoes steady-state (Hopf) bifurcations.

Lemma 2.1. *Let $d_3^*(\gamma)$ and $d_3^{**}(\gamma)$ be (2.11) and (2.12). Then the following results hold.*

- (i) $d_3^*(\gamma)$ is decreasing with γ , and crosses the origin for some n ; $d_3^{**}(\gamma)$ is increasing with γ for some n .
- (ii) $d_{3N}^{**}(\gamma) = \max d_3^*(\gamma) < 0$ and $d_{3M}^{**}(\gamma) = \min d_3^{**}(\gamma) > 0$ with $\gamma > 0$ and $N, M \in \mathbb{N}$.

Proof. (i) From (2.11), it follows that $d_3^*(\gamma)$ is a direct line with slope

$$k_n = -\frac{\alpha+1}{bm\alpha^2\mu_n} \left\{ \frac{sm\alpha}{\alpha+1} + [d_1 \mu_n - 1 + \beta\alpha + \frac{m\alpha}{(\alpha+1)^2}] [d_2 \mu_n - s + 2] \right\} < 0,$$

and (2.12) can be rewritten as

$$d_3^{**}(\gamma) = A_0 \gamma^2 + A_1 \gamma + A_2$$

with

$$\begin{aligned} A_0 &= \frac{\alpha+1}{bm\alpha^2\mu_n} [(d_1 + d_2)\mu_n + \beta\alpha + \frac{m\alpha}{(\alpha+1)^2} + 1 - s] = \frac{\alpha+1}{bm\alpha^2\mu_n} \{ [d_1 \mu_n - 1 + \beta\alpha + \frac{m\alpha}{(\alpha+1)^2}] + [d_2 \mu_n - s + 2] \}, \\ A_1 &= \frac{\alpha+1}{bm\alpha^2\mu_n} \{ [d_1 \mu_n - 1 + \beta\alpha + \frac{m\alpha}{(\alpha+1)^2}] + [d_2 \mu_n - s + 2] \}^2, \\ A_2 &= \frac{\alpha+1}{bm\alpha^2\mu_n} \left\{ [d_1 \mu_n - 1 + \beta\alpha + \frac{m\alpha}{(\alpha+1)^2}]^2 [d_2 \mu_n - s + 2] + [d_1 \mu_n - 1 + \beta\alpha + \frac{m\alpha}{(\alpha+1)^2}] [d_2 \mu_n - s + 2]^2 \right. \\ &\quad \left. + \frac{sm\alpha}{\alpha+1} \{ [d_1 \mu_n - 1 + \beta\alpha + \frac{m\alpha}{(\alpha+1)^2}] + [d_2 \mu_n - s + 2] \} \right\}. \end{aligned}$$

It follows that $A_0 > 0$, $A_1 > 0$, $A_2 > 0$ and let $\gamma = -\frac{A_0}{2A_1}$. Thus, $d_3^{**}(\gamma)$ is increasing for $\gamma > 0$. Since $d_3^{**}(0) = A_2 > 0$, then $d_3^{**}(\gamma) > 0$ for all $\gamma > 0$.

(ii) k_n attains its maximum due to the hook function. k_n can get to its maximum at $\bar{\mu}_n$. Take N as μ_N is eigenvalue closest for $\bar{\mu}_n$ and $d_{3N}^{**}(\gamma) < 0$ from (i).

Rewrite $d_3^{**}(\gamma)$ by expressing μ_n in terms of n :

$$d_3^{**}(\gamma) = \frac{\alpha + 1}{b\alpha^2 n} \left\{ A_n B_n - \frac{\gamma s \alpha}{\alpha + 1} - \gamma [d_1 n - 1 + \beta \alpha + \frac{m\alpha}{(\alpha + 1)^2}] [d_2 n - s + 2] \right\}. \quad (2.13)$$

Then we have

$$\begin{aligned} \frac{d[d_3^{**}(\gamma)]}{dn} &= -\frac{\alpha + 1}{b\alpha^2 n^2} \left\{ A_n B_n - \frac{\gamma s \alpha}{\alpha + 1} - \gamma [d_1 n - 1 + \beta \alpha + \frac{m\alpha}{(\alpha + 1)^2}] [d_2 n - s + 2] \right\} + \\ &\frac{\alpha + 1}{b\alpha^2 n} \left\{ -d_1 [d_2 n - s + 2] \gamma - [d_1 n - 1 + \beta \alpha + \frac{m\alpha}{(\alpha + 1)^2}] d_2 \gamma + [d_1 + d_2] B_n + A_n \{ [d_1 + d_2] \gamma + \right. \\ &\left. d_1 [d_2 n - s + 2] + [d_1 n - 1 + \beta \alpha + \frac{m\alpha}{(\alpha + 1)^2}] d_2 \right\} \right\} = -\frac{\alpha + 1}{b\alpha^2 n^2} A_3(n). \end{aligned}$$

Here, $A_3(n)$ is a cubic function in n . We verify that the equation $A_3(n) = 0$ has a unique positive root $n = n_*$. $A_3(n) > 0$ with $n \in (n_*, +\infty)$ and $A_3(n) < 0$ with $n \in (0, n_*)$. Thus, $d_3^{**}(\gamma)$ attains its minimum at $n = n_*$. Therefore, there must exist a positive integer M satisfying $d_{3M}^{**}(\gamma) = \min d_3^{**}(\gamma) > 0$. \square

Lemma 2.2. Let $d_{3N}^*(\gamma)$ and $d_{3M}^{**}(\gamma)$ be in Lemma 2.1. Then statements below hold.

- (i) All roots of the characteristic equation have negative real parts as $d_{3N}^*(\gamma) < d_3 < d_{3M}^{**}(\gamma)$.
- (ii) The characteristic equation has a pair of purely imaginary roots as $d_3 \geq d_{3M}^{**}(\gamma)$.
- (iii) The characteristic equation has a zero root as $d_3 \leq d_{3N}^*(\gamma)$.

Proof. By Lemma 2.1, when $d_{3N}^*(\gamma) < d_3 < d_{3M}^{**}(\gamma)$, it follows that $C_n > 0$, $A_n B_n - C_n > 0$ with $\mu_n > 0$; thus, (i) holds. If $d_3 \leq d_{3N}^*(\gamma)$, then $C_n < 0$, indicating that characteristic equation owns one positive real part eigenvalue. As $d_3 = d_{3M}^{**}(\gamma)$, the characteristic equation has a zero root. If $d_3 \geq d_{3M}^{**}(\gamma)$, then $A_n > 0$, $C_n > 0$, $A_n B_n - C_n < 0$, and the characteristic equation has a pair of purely imaginary roots with $d_3 = d_{3M}^{**}(\gamma)$. \square

Based on Lemma 2.2, we derive the following lemma.

Lemma 2.3. The characteristic equation has a pair of roots as $\lambda = \lambda(d_3) \pm i\omega(d_3)$ as d_3 is near $d_3^{**}(\gamma)$ with $\lambda(d_3^{**}(\gamma)) = 0$ and $\lambda'(d_3^{**}(\gamma)) > 0$.

Proof. Differentiating the characteristic equation with respect to d_3 , we get

$$3\lambda^2 \frac{d\lambda}{dd_3} + \frac{dA_n}{dd_3} \lambda^2 + 2\lambda A_n \frac{d\lambda}{dd_3} + \frac{dB_n}{dd_3} \lambda + B_n \frac{d\lambda}{dd_3} + \frac{dC_n}{dd_3} = 0. \quad (2.14)$$

From the equations of A_n , B_n , and C_n , we obtain

$$\frac{dA_n}{dd_3} = 0, \quad \frac{dB_n}{dd_3} = 0, \quad \frac{dC_n}{dd_3} = \frac{b\alpha^2}{\alpha + 1} \mu_n. \quad (2.15)$$

Let $\lambda = i\omega_n$, then get

$$\left. \frac{d\lambda}{dd_3} \right|_{d_3=d_3^{**}(\gamma)} = \frac{b\alpha^2 \mu_n}{(\alpha + 1)(3\omega_n^2 - B_n + 2iA_n\omega_n)}, \quad (2.16)$$

and

$$\lambda'(d_3) = \frac{b\alpha^2 \mu_n}{(\alpha + 1)((3\omega_n^2 - B_n)^2 - 4A_n^2\omega_n^2)} > 0.$$

\square

Combining with Lemmas 2.1–2.3, we have the following conclusions.

Theorem 2.3. Let $d_3^*(\gamma)$, $d_{3N}^{**}(\gamma)$ be (2.11) and (2.12), $d_{3N}^*(\gamma)$, $d_{3M}^{**}(\gamma)$ be in Lemma 2.1. Then results below are true with system (2.1).

- (i) n -mode Turing bifurcations occur at $d_3 = d_3^*(\gamma)$ with $\gamma > 0$, $n \in \mathbb{N}$; n -mode nonhomogeneous steady states appear near E^* .
- (ii) n -mode Hopf bifurcations occur at $d_3 = d_{3M}^{**}(\gamma)$ with $\gamma > 0$, $n \in \mathbb{N}$; nonhomogeneous periodic solutions appear near E^* .
- (iii) For some $\gamma \in (0, +\infty)$, E^* is locally stable with $d_{3N}^*(\gamma) < d_3 < d_{3M}^{**}(\gamma)$, and unstable with $d_3 \in (-\infty, d_{3N}^*(\gamma)] \cup [d_{3M}^{**}(\gamma), +\infty)$.

Remark 2.1. Biologically, Theorem 2.3 indicates that when consumers disperse based on local perception, the three populations might not settle into a homogeneous equilibrium but instead exhibit spatially heterogeneous patterns. This means population densities can differ across spatial regions. This indicates that system (2.1) undergoes a Turing bifurcation under the influence of the spatial memory diffusion coefficient, leading the system to transition from a homogeneous steady state to a stable spatial pattern, and consequently the population density exhibits spatial heterogeneity. Additionally, the emergence of spatially nonhomogeneous Hopf bifurcations suggests that populations may display not only periodic distributions but also spatial variations within these cycles.

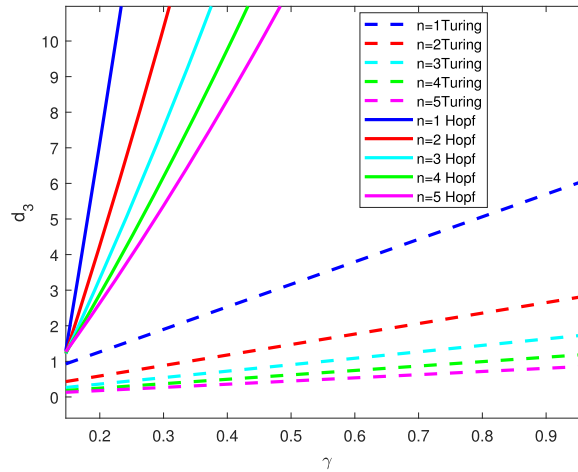


Fig. 1. The bifurcation diagram of (2.1) in (γ, d_3) plane.

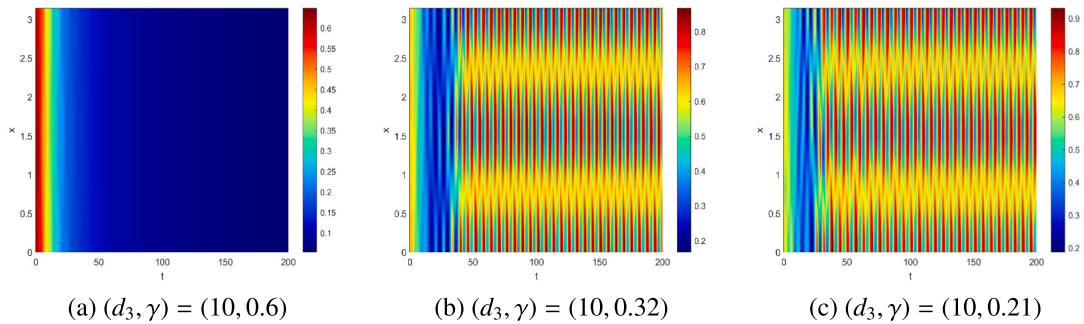


Fig. 2. Spatial periodic patterns of resources near the Hopf bifurcation curves in (2.1).

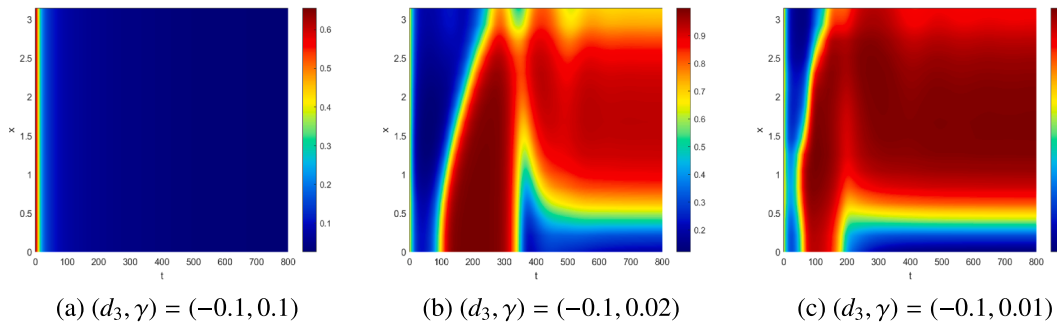


Fig. 3. Patterns of resources near the Turing bifurcation curves in (2.1).

Next, we present numerical simulations to validate the analytical results and to obtain ecological insights. According to [17] and the biological meanings, we set the parameters as follows: $\Omega = (0, \pi)$, $d_1 = 0.01$, $d_2 = 0.03$, $b = 0.15$, $m = 1$, $s = 0.1$, and $\beta = 1$. We illustrate only the resource distributions, as consumer distributions exhibit similar spatial patterns.

Fig. 1 displays several Turing and Hopf bifurcation curves. Hopf bifurcation curves corresponding to different modes may intersect, resulting in double Hopf bifurcations. For a fixed $d_3 = 10$, Fig. 2 shows that the homogeneous steady state E^* remains stable at $\gamma = 0.6$. As γ decreases to 0.32, a nonhomogeneous periodic pattern with mode 2 emerges. This pattern remains stable even at $\gamma = 0.21$. Consequently, the spatial distribution of resources exhibits temporally periodic variations.

Fig. 3 presents the spatially nonhomogeneous steady state along with selected Turing patterns. Fixing $d_3 = -0.1$, the constant steady state E^* remains stable at $\gamma = 0.1$. As γ decreases to 0.02, a nonhomogeneous steady state emerges, which continues to persist at $\gamma = 0.01$. This suggests that as the decay rate γ decreases, the stable homogeneous equilibrium transitions into an irregular bar-like pattern. Further reductions in γ result in the development of increasingly distinct bar patterns.

2.2. Dynamics of (2.2)

In this subsection, we analyze the stability and conditions of bifurcations in (2.2). Consider the constant equilibrium $E_* = (u_*, v_*, q_*) = (\alpha, \alpha, b\alpha^2/(\gamma + \xi\alpha))$, which is locally stable in non-spatial system of (2.2).

Linearizing (2.2) at E_* , we obtain

$$\hat{\mathbf{Q}} \begin{pmatrix} \phi \\ \psi \\ \varphi \end{pmatrix} = \begin{pmatrix} d_1 \Delta \phi + (1 - \beta\alpha - \frac{m\alpha}{(\alpha+1)^2})\phi - \frac{m\alpha}{\alpha+1}\psi \\ d_2 \Delta \psi - d_3 \alpha \Delta \varphi + s\phi + (s-2)\psi \\ b\alpha\phi + \frac{b\alpha\gamma}{\gamma+\xi\alpha}\psi - (\gamma + \xi\alpha)\varphi \end{pmatrix}, \quad (2.17)$$

where α is defined as previously. Thus, linear operator $\hat{\mathbf{Q}}$ is closed in Y , $D(\hat{\mathbf{Q}}) = X$. We now present spectral properties of $\hat{\mathbf{Q}}$.

Theorem 2.4. Denote $\hat{\mathbf{Q}} : X \rightarrow Y$. Spectrum of $\hat{\mathbf{Q}}$ is given by

$$\sigma(\hat{\mathbf{Q}}) = \sigma_p(\hat{\mathbf{Q}}) = \hat{S} \cup \{-\gamma - \xi\alpha\},$$

where

$$\hat{S} = \{\hat{\mu}_n^{(1)}\}_{n=0}^{+\infty} \cup \{\hat{\mu}_n^{(2)}\}_{n=0}^{+\infty} \cup \{\hat{\mu}_n^{(3)}\}_{n=0}^{+\infty}, \quad (2.18)$$

and $\hat{\mu}_n^{(j)}$ ($j = 1, 2, 3$) are roots of the characteristic equation:

$$\lambda^3 + \hat{A}_n \lambda^2 + \hat{B}_n \lambda + \hat{C}_n = 0,$$

satisfying $\Re(\hat{\mu}_n^{(1)}) < \Re(\hat{\mu}_n^{(2)}) < \Re(\hat{\mu}_n^{(3)})$. The coefficients are defined as

$$\begin{aligned} \hat{A}_n &= (d_1 + d_2)\mu_n + \beta\alpha + \frac{m\alpha}{(\alpha+1)^2} + 1 - s + \gamma + \xi\alpha, \\ \hat{B}_n &= [(d_1 + d_2)\mu_n + \beta\alpha + \frac{m\alpha}{(\alpha+1)^2} + 1 - s][\gamma + \xi\alpha] + [d_1\mu_n - 1 + \beta\alpha + \frac{m\alpha}{(\alpha+1)^2}][d_2\mu_n - s + 2] + \frac{sma}{\alpha+1} - \frac{\alpha^2 b\gamma d_3 \mu_n}{\gamma + \xi\alpha}, \\ \hat{C}_n &= [d_1\mu_n - 1 + \beta\alpha + \frac{m\alpha}{(\alpha+1)^2}][d_2\mu_n - s + 2][\gamma + \xi\alpha] - \frac{b\alpha^2 \gamma d_3 \mu_n}{\gamma + \xi\alpha} [d_1\mu_n - 1 + \beta\alpha + \frac{m\alpha}{(\alpha+1)^2}] \\ &\quad + \frac{d_3 b m \alpha^3}{\alpha+1} \mu_n + \frac{[\gamma + \xi\alpha]sma}{\alpha+1}. \end{aligned}$$

The proof of Theorem 2.4 is similar to that of Theorem 2.1 and is therefore omitted. This result establishes the stability of the system.

Theorem 2.5. E_* is locally stable in system (2.2) as all the roots of the characteristic equation own negative real parts; otherwise, it is unstable.

By Theorems 2.4–2.5, we derive steady state bifurcation points by setting $\hat{C}_n = 0$:

$$\hat{d}_3^*(\gamma) = \left\{ \frac{b\alpha^2 \gamma \mu_n}{\gamma + \xi\alpha} [d_1\mu_n - 1 + \alpha\beta + \frac{m\alpha}{(\alpha+1)^2}] - \frac{b m \alpha^3}{\alpha+1} \mu_n \right\}^{-1} \left\{ [d_1\mu_n - 1 + \beta\alpha + \frac{m\alpha}{(\alpha+1)^2}][d_2\mu_n - s + 2][\gamma + \xi\alpha] + \frac{[\gamma + \xi\alpha]sma}{\alpha+1} \right\}. \quad (2.19)$$

Similarly, from $\hat{A}_n \hat{B}_n - \hat{C}_n = 0$, we obtain:

$$\hat{d}_3^{**}(\gamma) = \left\{ \frac{b\alpha^2 \gamma \mu_n}{\gamma + \xi\alpha} [d_1\mu_n - 1 + \alpha\beta + \frac{m\alpha}{(\alpha+1)^2}] - \frac{b m \alpha^3}{\alpha+1} \mu_n \right\}^{-1} \left\{ [d_1\mu_n - 1 + \beta\alpha + \frac{m\alpha}{(\alpha+1)^2}][d_2\mu_n - s + 2][\gamma + \xi\alpha] + \frac{[\gamma + \xi\alpha]sma}{\alpha+1} + \hat{A}_n \hat{B}_n \right\}. \quad (2.20)$$

Similarly, (2.19) ((2.20)) indicates that the consumers can attract toward regions of lower (higher) population density, then system (2.2) undergoes steady-state (Hopf) bifurcations. In what follows, we analyze the properties of the Turing curves $d_3 = \hat{d}_3^*(\gamma)$.

Lemma 2.4. Let $\hat{d}_3^*(\gamma)$ and $\hat{d}_3^{**}(\gamma)$ be (2.19) and (2.20). Then results below hold.

- (i) There exist n^* such that $n \leq n^*$, $\hat{d}_3^*(\gamma) < 0$, and for an integer \hat{N} where $d_{3\hat{N}}^*(\gamma) = \max \hat{d}_3^*(\gamma)$ with some $\gamma > 0$; For $n > n^*$, $\hat{d}_3^*(\gamma) < 0$ when $\gamma \in (0, \gamma_n^*)$, and $\hat{d}_3^*(\gamma) > 0$ when $\gamma \in (\gamma_n^*, +\infty)$, where γ_n^* satisfies $\frac{1}{d_{3\hat{N}}^*(\gamma_n^*)} = 0$. Moreover, $\hat{d}_3^*(\gamma)$ is strictly decreasing in n for fixed γ and satisfies:

$$\hat{d}_3^*(\gamma) > \hat{d}_{3\infty}^*(\gamma) = \frac{d_2[\gamma + \xi\alpha]^2}{b\alpha^2 \gamma}, \quad (2.21)$$

where $\hat{d}_{3\infty}^*(\gamma)$ decreases as $\gamma \in (0, \gamma^*)$ and increases as $\gamma \in (\gamma^*, +\infty)$ with $\gamma^* = \alpha\xi$.

- (ii) $d_{3\hat{M}}^{**}(\gamma) = \min \hat{d}_3^{**}(\gamma)$ for fixed $\gamma > 0$ and $\hat{M} \in \mathbb{N}$.

Similarly we can obtain the properties of eigenvalues of the characteristic equation below.

Lemma 2.5. Let $\hat{d}_3^*(\gamma)$ and $\hat{d}_3^{**}(\gamma)$ be defined as in (2.19) and (2.20), with $d_{3N}^*(\gamma)$ and $d_{3M}^{**}(\gamma)$ as in Lemma 2.4. Then conclusions below hold.

- (i) For $d_{3N}^*(\gamma) < d_3 < \min\{d_{3M}^{**}(\gamma), \hat{d}_{3\infty}^*(\gamma)\}$, all eigenvalues of the characteristic equation own negative real parts.
- (ii) For $d_3 \geq \min\{d_{3M}^{**}(\gamma), \hat{d}_{3\infty}^*(\gamma)\}$, the characteristic equation owns a pair of purely imaginary roots when $d_3 = \hat{d}_3^{**}(\gamma)$.
- (iii) For $d_3 \leq d_{3N}^*(\gamma)$ or $d_3 \geq \min\{d_{3M}^{**}(\gamma), \hat{d}_{3\infty}^*(\gamma)\}$, the characteristic equation has a zero root at $d_3 = \hat{d}_3^*(\gamma)$.

Remark 2.2. Lemma 2.4 implies that when the homogeneous steady state loses stability at $d_3 = \hat{d}_{3\infty}^*(\gamma)$, the corresponding linearized system has infinitely many eigenvalues with positive real parts. Therefore, the system becomes unstable, and periodic temporal oscillations will occur.

Next, we verify the transversality condition for Hopf bifurcation in (2.2) and omit the proof.

Lemma 2.6. The characteristic equation has a pair of roots as $\hat{\lambda} = \hat{\lambda}(d_3) \pm i\hat{\omega}(d_3)$ near $d_3 = \hat{d}_3^{**}(\gamma)$ satisfying $\hat{\lambda}(\hat{d}_3^{**}(\gamma)) = 0$ and $\hat{\lambda}'(\hat{d}_3^{**}(\gamma)) > 0$.

By Lemmas 2.4–2.6, we obtain stability and bifurcations of E_* in system (2.2).

Theorem 2.6. Let $\hat{d}_3^*(\gamma)$, $\hat{d}_3^{**}(\gamma)$, $d_{3N}^*(\gamma)$, and $d_{3M}^{**}(\gamma)$ be as defined above. Then in system (2.2)

- (i) n -mode Turing bifurcations occur at $d_3 = d_{3N}^*(\gamma)$ with $\gamma > 0$, $n \in \mathbb{N}$, leading to spatially nonhomogeneous steady states near E_* ;
- (ii) n -mode Hopf bifurcations occur at $d_3 = d_{3M}^{**}(\gamma)$ with $\gamma > 0$, $n \in \mathbb{N}$, generating spatially nonhomogeneous periodic solutions near E_* ;
- (iii) for some $\gamma \in (0, +\infty)$, E_* is locally stable if $d_{3N}^*(\gamma) < d_3 < \min\{d_{3M}^{**}(\gamma), \hat{d}_{3\infty}^*(\gamma)\}$; and unstable if $d_3 \in (-\infty, d_{3N}^*(\gamma)) \cup [\min\{d_{3M}^{**}(\gamma), \hat{d}_{3\infty}^*(\gamma)\}, +\infty)$.

In the following simulations, set $\Omega = (0, \pi)$ with parameters $d_1 = 0.01$, $d_2 = 0.02$, $b = 0.15$, $s = 0.1$, $\xi = 0.3$, $\beta = 1$. The resource distributions are shown similarly for consumers except Fig. 9.

Fig. 4 displays Turing and Hopf bifurcation curves, revealing several key features: The limiting Turing bifurcation curve $d_3 = \hat{d}_{3\infty}^*(\gamma)$ corresponds to infinite modes and destabilises system (2.2) when $d_3 > \hat{d}_{3\infty}^*(\gamma)$. Intersections between different Hopf bifurcation modes indicate the occurrence of double Hopf bifurcations.

For the specific case $d_3 = 1$, in Fig. 5 the steady state E_* becomes unstable at $\gamma = 0.09$, giving rise to 5-mode quasi-periodic patterns. When γ decreases to 0.08, 4-mode nonhomogeneous periodic pattern emerges. This 4-mode pattern persists but remains unstable at $\gamma = 0.05$.

These results directly indicate that the spatial resource distributions undergo periodic temporal oscillations under the influence of smaller decay rate. When the local perception decay is not obvious, distributions of resources and consumers present a periodic distribution, but the distribution range is large. Once the local perception decay is very serious, distributions of resources and consumers still oscillate periodically, but due to the weak local perception memory, distributions of resources and consumers are not concentrated.

Choose $d_3 = 1$, $\gamma = 0.1$, $m = 0.8$. Fig. 6 shows that the decay rate associated with consumers returning to areas with low resource density ξ can influence the dynamics of (2.2). The dynamics exhibit strong dependence on ξ . At $\xi = 0.3$, 5-mode periodic patterns emerge. At $\xi = 0.4$, system stabilizes to constant resource-consumer distributions. This indicates that the density distributions of resources and consumers eventually reach a steady state with the enhancement of resource memory decay.

In Figs. 7–8, some patterns near Hopf bifurcation curves are investigated by varying m . Fix $m = 0.8$, $\gamma = 0.1$, as $d_3 = 0.9$, a quasi-periodic pattern occurs. While d_3 decreases to 0.8, then resources and consumers coexist. Fix $(d_3, \gamma) = (1, 0.1)$, a quasi-periodic pattern occurs with $m = 0.7$; increase m to 0.8, then there are 5-mode nonhomogeneous periodic patterns. If $m = 0.9$, then 4-mode nonhomogeneous periodic pattern remains unstable. Finally, resources and consumers coexist and are stable with $m = 1$. This shows that with the continuous full contact between consumers and resources, they eventually show a steady state distribution.

Fig. 9 demonstrates the emergence of spatially nonhomogeneous steady states and Turing patterns with $d_3 = 1$, $\gamma = 0.1$. Key observations reveal pattern formations. The homogeneous steady state E_* becomes unstable at $m = 1.1$. Resources and implicit memory maintain an even spatial distribution. Consumers develop coexisting dot and stripe patterns. Frequent resource-consumer interactions lead to various system dynamics. Stable distributions are displayed for both resources and implicit memory. Persistent coexistence of dot and bar patterns occur for consumers. These phenomena are notably absent in system (2.1), highlighting the distinctive dynamics of system (2.2). Compared to [17], it shows that systems (2.1)–(2.2) with local perception have similar results, both Hopf and Turing bifurcations are caused by the cognitive diffusion, and populations presents complex patterns.

3. Dynamics with nonlocal perception

In this part, we study stability and conditions of bifurcations for systems (1.1)–(1.2) in the presence of nonlocality, and demonstrate corresponding results by simulations.

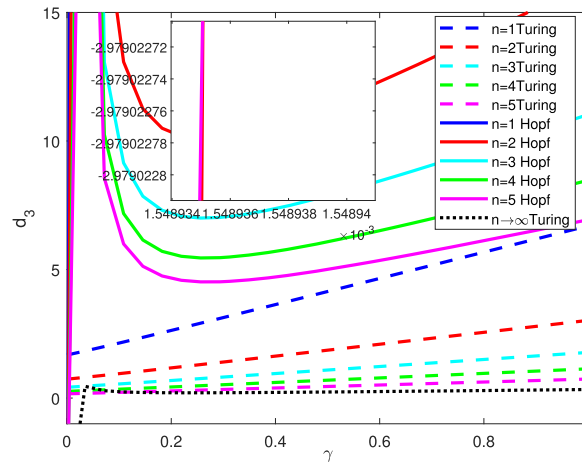


Fig. 4. The bifurcation diagram of (2.2) in (γ, d_3) plane.

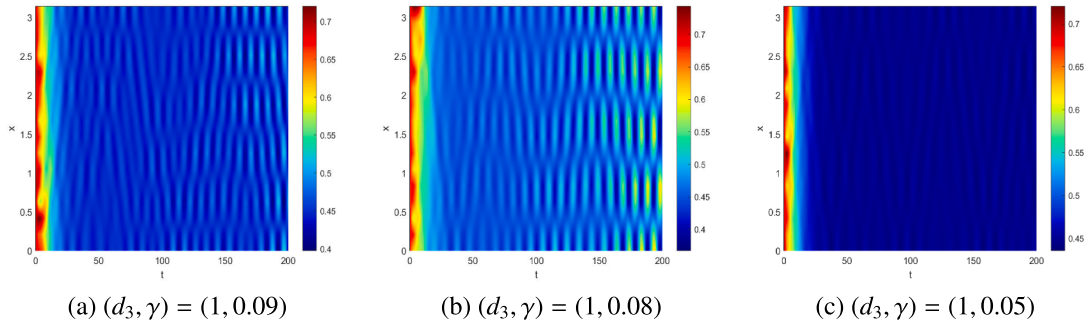


Fig. 5. Spatially periodic resource patterns near the Hopf bifurcation curves of (2.2).

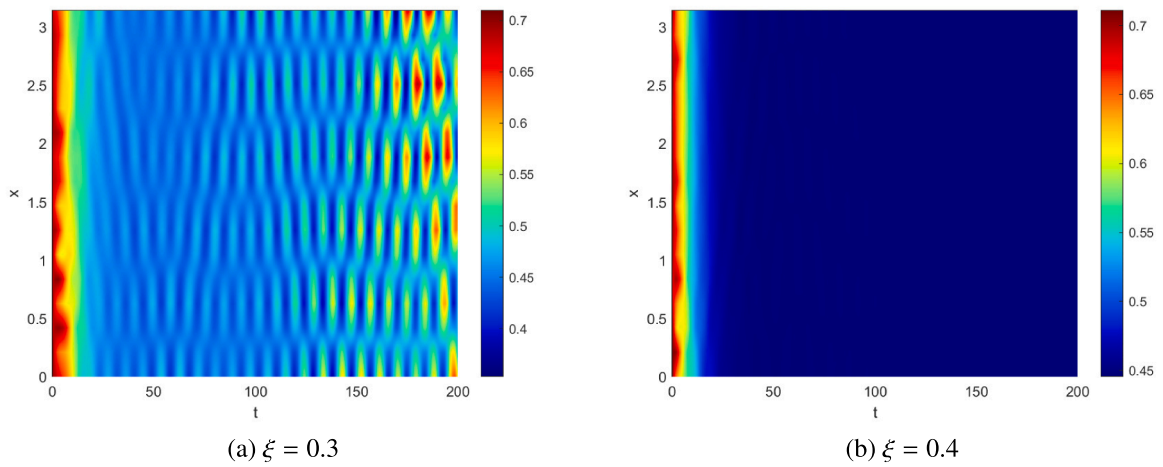


Fig. 6. Resource patterns near Hopf bifurcation curves of (2.2).

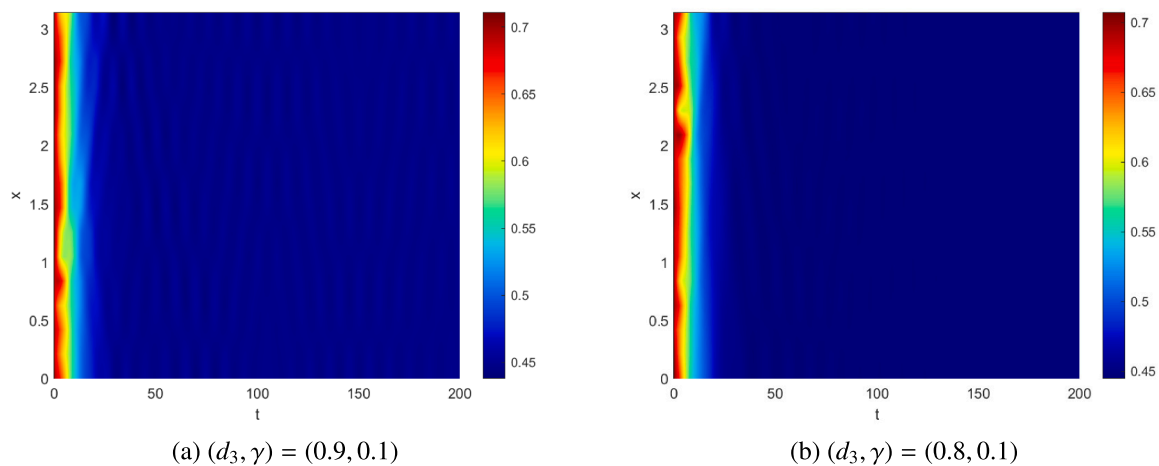


Fig. 7. Fix $m = 0.8$. patterns of resources near the Hopf bifurcation curves of (2.2).

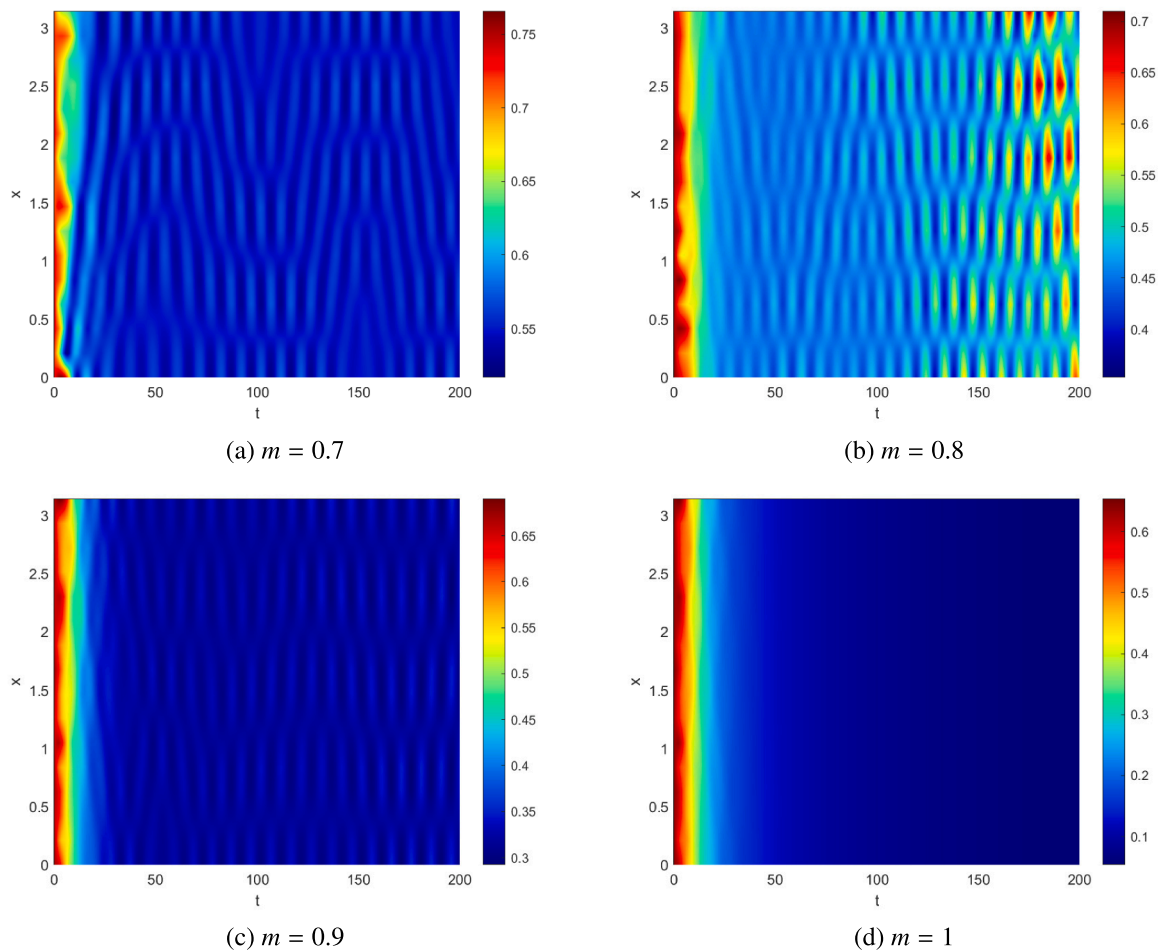


Fig. 8. Periodic patterns of resources near the Hopf bifurcation curves of (2.2).

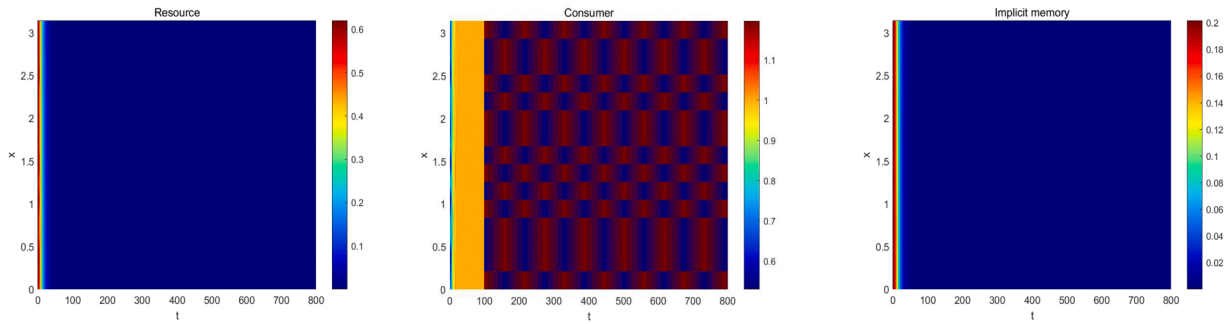


Fig. 9. Spatially nonhomogeneous patterns populations near Turing bifurcation curves of (2.2).

3.1. Dynamics of (1.1)

This subsection focuses on investigating dynamics of system (1.1). It still possesses the constant equilibrium E^* . The linearized system at E^* is derived below:

$$\frac{\partial}{\partial t} \begin{pmatrix} u \\ v \\ q \end{pmatrix} = D_1 \Delta \begin{pmatrix} u \\ v \\ q \end{pmatrix} + \bar{A} \begin{pmatrix} u \\ v \\ q \end{pmatrix} + B \begin{pmatrix} \hat{u} \\ \hat{v} \\ \hat{q} \end{pmatrix},$$

where

$$\bar{A} = \begin{pmatrix} 1 - \beta\alpha - \frac{m\alpha}{(\alpha+1)^2} & -\frac{m\alpha}{\alpha+1} & 0 \\ s & s-2 & 0 \\ 0 & 0 & -\gamma \end{pmatrix}, \quad B = \begin{pmatrix} 0 & 0 & 0 \\ 0 & 0 & 0 \\ b & 0 & 0 \end{pmatrix}.$$

The characteristic equation is

$$\lambda^3 + A_n \lambda^2 + B_n \lambda + C_{n1} = 0, \quad (3.1)$$

where

$$C_{n1} = \gamma[d_1\mu_n - 1 + \beta\alpha + \frac{m\alpha}{(\alpha+1)^2}][d_2\mu_n - s + 2] + \frac{d_3 b m \alpha^2}{\alpha+1} H(R, n) \mu_n + \frac{\gamma s m \alpha}{\alpha+1},$$

$$H(R, n) = \begin{cases} \frac{\sin(nR)}{nR}, & n \neq 0, \\ 1, & n = 0. \end{cases}$$

For $n = 0$, Eq. (3.1) reduces to the characteristic equation of the corresponding ODE of (1.1) at E^* . Under the conditions of (2.4), E^* remains stable. When $R = 0$, $H(0, n) = 1$ for $n \neq 0$, $n \in \mathbb{R}$, and the characteristic equation simplifies to that of (2.1) without nonlocal perception. The analysis below focuses on the case where $n > 0$ and $R > 0$, exploring the distribution of roots of (3.1). Note that changes in the stability of E^* and potential bifurcations are linked to characteristic roots with zero real parts. Since the perception scale R can influence the value of C_{n1} , it may also affect the stability of E^* and the occurrence of bifurcations.

To analyze the spectrum, we define the following spaces:

$$X = W_N^{2,p}(\Omega) \times W_N^{2,p}(\Omega) \times W^{2,p}(\Omega), \quad Y = L^p(\Omega) \times L^p(\Omega) \times W_N^{2,p}(\Omega)$$

with

$$W_N^{2,p}(\Omega) = \{u \in W^{2,p}(\Omega) : \partial_n u = 0 \text{ on } \partial\Omega\}.$$

From the linearization process, we obtain the linear operator:

$$\bar{\mathfrak{L}} \begin{pmatrix} \phi \\ \psi \\ \varphi \end{pmatrix} = \begin{pmatrix} d_1 \Delta \phi + (1 - \beta\alpha - \frac{m\alpha}{(\alpha+1)^2})\phi - \frac{m\alpha}{\alpha+1}\psi \\ d_2 \Delta \psi - d_3 \alpha \Delta \varphi + s\phi + (s-2)\psi \\ -\gamma\varphi \end{pmatrix}, \quad (3.2)$$

where closed linear operator $\bar{\mathfrak{L}}$ satisfies $D(X) = \bar{\mathfrak{L}}$. This implies $\phi, \psi \in W_N^{2,p}(\Omega)$, and $\varphi \in W^{2,p}(\Omega)$. Based on [28], we derive the following results.

Theorem 3.1. Spectrum of $\bar{\mathfrak{L}}$ is given by:

$$\sigma(\bar{\mathfrak{L}}) = \sigma_p(\bar{\mathfrak{L}}) = S \cup \{-\gamma\},$$

here

$$S = \{\mu_n^{(1)}\}_{n=0}^{+\infty} \cup \{\mu_n^{(2)}\}_{n=0}^{+\infty} \cup \{\mu_n^{(3)}\}_{n=0}^{+\infty}, \quad (3.3)$$

and $\mu_n^{(j)} (j = 1, 2, 3)$ are the characteristic roots satisfying $\Re(\mu_n^{(1)}) < \Re(\mu_n^{(2)}) < \Re(\mu_n^{(3)})$.

Proof. Consider the nonhomogeneous problem:

$$\begin{cases} d_1 \Delta \phi + (1 - \beta \alpha - \frac{m\alpha}{(\alpha+1)^2})\phi - \frac{m\alpha}{\alpha+1}\psi = \mu\phi + \tau_1, \\ d_2 \Delta \psi - d_3 \alpha \Delta \varphi + s\phi + (s-2)\psi = \mu\psi + \tau_2, \\ -\gamma\varphi = \mu\varphi + \tau_3, \\ \partial_n \phi = \partial_n \psi = 0, \end{cases} \quad (3.4)$$

where $\mu \in \mathbb{C}$ and $(\tau_1, \tau_2, \tau_3) \in Y$.

Case 1 $\mu + \gamma \neq 0$.

The system (3.4) simplifies to:

$$\begin{cases} d_1 \Delta \phi + (1 - \beta \alpha - \frac{m\alpha}{(\alpha+1)^2})\phi - \frac{m\alpha}{\alpha+1}\psi = \mu\phi + \tau_1, \\ d_2 \Delta \psi + \frac{d_3 \alpha}{\mu + \gamma} \Delta \tau_3 + s\phi + (s-2)\psi = \mu\psi + \tau_2, \\ \partial_n \phi = \partial_n \psi = 0. \end{cases}$$

Equivalently,

$$\tilde{\mathfrak{L}}_1 \begin{pmatrix} \phi \\ \psi \end{pmatrix} = \begin{pmatrix} d_1 \Delta \phi + (1 - \beta \alpha - \frac{m\alpha}{(\alpha+1)^2})\phi - \frac{m\alpha}{\alpha+1}\psi - \mu\phi \\ d_2 \Delta \psi + s\phi + (s-2)\psi - \mu\psi \end{pmatrix} = \begin{pmatrix} \tau_1 \\ \tau_2 - \frac{d_3 \alpha}{\mu + \gamma} \Delta \tau_3 \end{pmatrix}. \quad (3.5)$$

Assume $\phi, \psi \in W_N^{2,p}(\Omega)$ and express them as:

$$\phi = \sum_{n=0}^{+\infty} a_n \phi_n, \quad \psi = \sum_{n=0}^{+\infty} b_n \phi_n. \quad (3.6)$$

Substituting (3.6) into (3.5) and integrating yields:

$$\begin{pmatrix} -d_1 \lambda_n + (1 - \beta \alpha - \frac{m\alpha}{(\alpha+1)^2}) - \mu & -\frac{m\alpha}{\alpha+1} \\ s & -d_2 \lambda_n + s - 2 - \mu \end{pmatrix} \begin{pmatrix} a_n \\ b_n \end{pmatrix} = \begin{pmatrix} \int_0^{l\pi} \tau_1 dx \\ \int_0^{l\pi} (\tau_2 - \frac{d_3 \alpha}{\mu + \gamma} \Delta \tau_3) dx \end{pmatrix}.$$

For $\tau_1 = \tau_2 = \tau_3 = 0$, the kernel satisfies $\text{Ker}(\tilde{\mathfrak{L}}_1) = \{(0, 0)^T\}$ and $\text{Ker}(\tilde{\mathfrak{L}} - \mu I)$ is $\{(0, 0, 0)^T\}$. Since it is injective, we have:

$$\begin{vmatrix} -d_1 \lambda_n + (1 - \beta \alpha - \frac{m\alpha}{(\alpha+1)^2}) - \mu & -\frac{m\alpha}{\alpha+1} \\ s & -d_2 \lambda_n + s - 2 - \mu \end{vmatrix} \neq 0,$$

which simplifies to:

$$(\mu + d_1 \lambda_n - (1 - \beta \alpha - \frac{m\alpha}{(\alpha+1)^2}))(\mu + 2 - s + d_2 \lambda_n) + \frac{sm\alpha}{\alpha+1} \neq 0. \quad (3.7)$$

(3.7) implies that $\tilde{\mathfrak{L}} - \mu I$ is surjective. It is also bijective. Moreover, $(\tilde{\mathfrak{L}} - \mu I)^{-1}$ is bounded, satisfying:

$$\|\phi\|_{W_N^{2,p}(\Omega)} + \|\psi\|_{W_N^{2,p}(\psi)} \leq \|(\tilde{\mathfrak{L}} - \mu I)^{-1}\| \left(\|d_1 \Delta \phi + 1 - \beta \alpha - \frac{m\alpha}{(\alpha+1)^2} \phi - \frac{m\alpha}{\alpha+1} \psi\|_{L^p(\Omega)} + \|d_2 \Delta \psi + s\phi + (s-2)\psi\|_{L^p(\Omega)} \right).$$

Thus, μ is in resolvent set of $\tilde{\mathfrak{L}}$, otherwise not in as (3.7) holds. If (3.7) fails, then the characteristic equation yields three roots $\mu_n^{(j)} (j = 1, 2, 3)$ $n \in \mathbb{N}_0$. Setting $\tau_j = 0 (j = 1, 2, 3)$ and substituting $\mu_n^{(j)}$ into (3.4), we obtain

$$\begin{pmatrix} \phi \\ \psi \\ \varphi \end{pmatrix} = \begin{pmatrix} \phi^{(j)} \\ \psi^{(j)} \\ \varphi^{(j)} \end{pmatrix} = \begin{pmatrix} 1 \\ \frac{\alpha+1}{m\alpha} [-d_1 \lambda_n - \mu_n^{(j)} + \frac{m\alpha}{(\alpha+1)^2} + \alpha\beta - 1] \\ 0 \end{pmatrix} \phi_n,$$

which shows that $\text{Ker}(\tilde{\mathfrak{L}} - \mu_n^{(j)}) = \text{Span}\{(\phi^{(j)}, \psi^{(j)}, \varphi^{(j)})^T\}$. Hence, $\mu_n^{(j)} (j = 1, 2, 3)$ are eigenvalues of $\tilde{\mathfrak{L}}$, $\mu_n^{(j)} \in \sigma_p(\tilde{\mathfrak{L}})$.

Case 2 $\mu + \gamma = 0$.

(3.4) reduces to:

$$\begin{cases} \psi = -\frac{\alpha+1}{b m \alpha} b \tau_1, \\ \Delta \varphi = \frac{1}{\alpha d_3} [d_2 \Delta \psi + (s-2+\gamma)\psi - \tau_2]. \end{cases}$$

For $\tau_i = 0 (i = 1, 2, 3)$, we find $\Re \text{er}(\tilde{\mathfrak{L}} + \gamma I) = \text{Span}\{(0, 0, \tilde{\varphi})^T\}$ for $\Delta \tilde{\varphi} = 0$, confirming $-\gamma \in \sigma_p(\tilde{\mathfrak{L}})$. This completes the proof. \square

Based on Theorem 3.1, we have the following theorem.

Theorem 3.2. The equilibrium E^* of system (1.1) is locally stable if all roots of characteristic equation own negative real parts; otherwise, it is unstable.

To analyze bifurcations, we use the Routh-Hurwitz criteria: eigenvalues own negative real parts iff

$$A_n > 0; C_{n1} > 0; A_n B_n - C_{n1} > 0.$$

Otherwise, system (1.1) undergoes bifurcations. Below, we discuss bifurcation conditions for different cases, taking the cognitive diffusion d_3 as the bifurcation parameter.

From $C_{n1} = 0$:

$$\bar{d}_3^*(\gamma) = -\frac{\alpha+1}{b\alpha^2\mu_n H(R,n)} \left\{ \frac{\gamma s\alpha}{\alpha+1} + [d_1\mu_n - 1 + \beta\alpha + \frac{m\alpha}{(\alpha+1)^2}] [d_2\mu_n - s + 2]\gamma \right\}. \quad (3.8)$$

From $A_n B_n - C_{n1} = 0$:

$$\bar{d}_3^{**}(\gamma) = \frac{\alpha+1}{b\alpha^2\mu_n H(R,n)} \left\{ A_n B_n - \frac{\gamma s\alpha}{\alpha+1} - [d_1\mu_n - 1 + \beta\alpha + \frac{m\alpha}{(\alpha+1)^2}] [d_2\mu_n - s + 2]\gamma \right\}, \quad (3.9)$$

By (2.4), $B_n > 0$ holds.

Lemma 3.1. Let $\bar{d}_3^*(\gamma)$ and $\bar{d}_3^{**}(\gamma)$ be defined as in (3.8) and (3.9). Then

- (i) $\bar{d}_3^*(\gamma)$ decreases in γ and crosses the origin for some n ; $\bar{d}_3^{**}(\gamma)$ increases in γ with some $n \in (2k\pi/R, (2k+1)\pi/R)$, $k \in \mathbb{N}$;
- (ii) for $n \in (2k\pi/R, (2k+1)\pi/R)$ ($k \in \mathbb{N}$) and $\gamma > 0$, there exist $N, M \in \mathbb{N}$ with

$$\bar{d}_{3N}^{**}(\gamma) = \max \bar{d}_3^*(\gamma) < 0 \text{ and } \bar{d}_{3M}^{**}(\gamma) = \min \bar{d}_3^{**}(\gamma) > 0.$$

Proof. (i) From (3.8), $\bar{d}_3^*(\gamma)$ is a direct line with slope

$$\bar{k}_n = -\frac{\alpha+1}{b\alpha^2\mu_n H(R,n)} \left\{ \frac{s\alpha}{\alpha+1} + [d_1\mu_n - 1 + \beta\alpha + \frac{m\alpha}{(\alpha+1)^2}] [d_2\mu_n - s + 2] \right\} < 0$$

for $n \in (2k\pi/R, (2k+1)\pi/R)$ ($k \in \mathbb{N}$).

Rewriting (3.9) as a quadratic in γ

$$\bar{d}_3^{**}(\gamma) = \bar{A}_0\gamma^2 + \bar{A}_1\gamma + \bar{A}_2$$

with

$$\begin{aligned} \bar{A}_0 &= \frac{\alpha+1}{b\alpha^2\mu_n H(R,n)} [(d_1+d_2)\mu_n + \beta\alpha + \frac{m\alpha}{(\alpha+1)^2} + 1 - s] = \frac{\alpha+1}{b\alpha^2\mu_n H(R,n)} \{ [d_1\mu_n - 1 + \beta\alpha + \frac{m\alpha}{(\alpha+1)^2}] + [d_2\mu_n - s + 2] \}, \\ \bar{A}_1 &= \frac{\alpha+1}{b\alpha^2\mu_n H(R,n)} \{ [d_1\mu_n - 1 + \beta\alpha + \frac{m\alpha}{(\alpha+1)^2}] + [d_2\mu_n - s + 2] \}^2, \bar{A}_2 = \frac{\alpha+1}{b\alpha^2\mu_n H(R,n)} \{ [d_1\mu_n - 1 + \beta\alpha + \frac{m\alpha}{(\alpha+1)^2}] \\ &+ [d_2\mu_n - s + 2] \} \frac{s\alpha}{\alpha+1} = \frac{s}{b\alpha\mu_n H(R,n)} \{ [d_1\mu_n - 1 + \beta\alpha + \frac{m\alpha}{(\alpha+1)^2}] + [d_2\mu_n - s + 2] \}. \end{aligned}$$

Clearly, $\bar{A}_0 > 0$, $\bar{A}_1 > 0$, $\bar{A}_2 > 0$ and $\gamma = -\frac{\bar{A}_0}{2\bar{A}_1}$ with $n \in (2k\pi/R, (2k+1)\pi/R)$ ($k \in \mathbb{N}$). Then $\bar{d}_3^{**}(\gamma)$ increases with $\gamma > 0$. Since $\bar{d}_3^{**}(0) = \bar{A}_2 > 0$, then $\bar{d}_3^{**}(\gamma) > 0$, $\gamma > 0$ with $n \in (2k\pi/R, (2k+1)\pi/R)$, $k \in \mathbb{N}$.

(ii) \bar{k}_n attains its maximum due to the properties of the hook function. Let $\bar{\mu}_n$ be the point where \bar{k}_n is maximized. Take N and μ_N is eigenvalue closest to $\bar{\mu}_n$, ensuring $\bar{d}_{3N}^{**}(\gamma) < 0$ from (i).

Rewriting $\bar{d}_3^{**}(\gamma)$ in terms of n (replacing μ_n into n):

$$\bar{d}_3^{**}(\gamma) = \frac{\alpha+1}{b\alpha^2 n H(R,n)} \left\{ A_n B_n - \frac{\gamma s\alpha}{\alpha+1} - [d_1 n - 1 + \beta\alpha + \frac{m\alpha}{(\alpha+1)^2}] [d_2 n - s + 2]\gamma \right\}. \quad (3.10)$$

Differentiating with respect to n :

$$\begin{aligned} \frac{d[\bar{d}_3^{**}(\gamma)]}{dn} &= -\frac{\alpha+1}{b\alpha^2 n^2 H(R,n)} \left\{ A_n B_n - \frac{\gamma s\alpha}{\alpha+1} - [d_1 n - 1 + \beta\alpha + \frac{m\alpha}{(\alpha+1)^2}] [d_2 n - s + 2]\gamma \right\} + \\ &\frac{\alpha+1}{b\alpha^2 n H(R,n)} \left\{ -d_1 [d_2 n - s + 2]\gamma - [d_1 n - 1 + \beta\alpha + \frac{m\alpha}{(\alpha+1)^2}] d_2 \gamma + [d_1 + d_2] B_n + A_n \{ [d_1 + d_2]\gamma + \right. \\ &\left. d_1 [d_2 n - s + 2] + [d_1 n - 1 + \beta\alpha + \frac{m\alpha}{(\alpha+1)^2}] d_2 \} \right\} = -\frac{\alpha+1}{b\alpha^2 n^2 H(R,n)} \bar{A}_3(n). \end{aligned}$$

Here $\bar{A}_3(n)$ is a cubic function of n . The equation $\bar{A}_3(n) = 0$ has a unique positive root $n = n_*$. $\bar{A}_3(n) > 0$ for $n \in (n_*, +\infty)$ and $\bar{A}_3(n) < 0$ for $n \in (0, n_*)$. Thus, $\bar{d}_3^{**}(\gamma)$ attains its minimum at $n = n_*$. Therefore, there exists a positive integer M such that $\bar{d}_{3M}^{**}(\gamma) = \min \bar{d}_3^{**}(\gamma) > 0$. \square

Lemma 3.2. Let $\bar{d}_{3N}^{**}(\gamma)$ and $\bar{d}_{3M}^{**}(\gamma)$ be defined as in Lemma 3.1 for $n \in (2k\pi/R, (2k+1)\pi/R)$ ($k \in \mathbb{N}$). Then

- (i) all roots of the characteristic equation have negative real parts if $\bar{d}_{3N}^{**}(\gamma) < d_3 < \bar{d}_{3M}^{**}(\gamma)$;
- (ii) the characteristic equation has a pair of purely imaginary roots if $d_3 \geq \bar{d}_{3M}^{**}(\gamma)$;
- (iii) the characteristic equation has a zero root if $d_3 \leq \bar{d}_{3N}^{**}(\gamma)$.

Proof. By Lemma 3.1, for $n \in (2k\pi/R, (2k+1)\pi/R)$ ($k \in \mathbb{N}$), if $\bar{d}_{3N}^{**}(\gamma) < d_3 < \bar{d}_{3M}^{**}(\gamma)$, then $C_{n1} > 0$, and $A_n B_n - C_{n1} > 0$ for $\mu_n > 0$, which validates (i). When $d_3 \leq \bar{d}_{3N}^{**}(\gamma)$, $C_{n1} < 0$, and the characteristic equation has at least one eigenvalue with positive real part. For $d_3 = \bar{d}_{3N}^{**}(\gamma)$, the characteristic equation has a zero root. If $d_3 \geq \bar{d}_{3M}^{**}(\gamma)$, then $A_n > 0$, $C_{n1} > 0$, and $A_n B_n - C_{n1} < 0$, causing the characteristic equation to have a pair of purely imaginary roots when $d_3 = \bar{d}_{3M}^{**}(\gamma)$. \square

From Lemma 3.2, the following lemma holds.

Lemma 3.3. The characteristic equation owns a pair of roots $\tilde{\lambda} = \tilde{\lambda}(d_3) \pm i\tilde{\omega}(d_3)$ when d_3 is near $\bar{d}_3^{**}(\gamma)$, with $\tilde{\lambda}(\bar{d}_3^{**}(\gamma)) = 0$ and $\tilde{\lambda}'(\bar{d}_3^{**}(\gamma)) > 0$ for some $n \in (2k\pi/R, (2k+1)\pi/R)$ ($k \in \mathbb{N}$).

Proof. Differentiating the characteristic equation with respect to d_3 yields

$$3\lambda^2 \frac{d\lambda}{dd_3} + \frac{dA_n}{dd_3} \lambda^2 + 2\lambda A_n \frac{d\lambda}{dd_3} + \frac{dB_n}{dd_3} \lambda + B_n \frac{d\lambda}{dd_3} + \frac{dC_{n1}}{dd_3} = 0. \quad (3.11)$$

From the equations of A_n, B_n, C_{n1} , then we obtain

$$\frac{dA_n}{dd_3} = 0, \quad \frac{dB_n}{dd_3} = 0, \quad \frac{dC_{n1}}{dd_3} = \frac{b\alpha^2}{\alpha+1} H(R, n) \mu_n. \quad (3.12)$$

Let $\lambda = i\omega_n$, then get

$$\left. \frac{d\lambda}{dd_3} \right|_{d_3=\bar{d}_3^{**}(\gamma)} = \frac{b\alpha^2 H(R, n) \mu_n}{(\alpha+1)(3\omega_n^2 - B_n + 2iA_n \omega_n)}, \quad (3.13)$$

and

$$\lambda'(d_3) = \frac{b\alpha^2 H(R, n) \mu_n}{(\alpha+1)((3\omega_n^2 - B_n)^2 - 4A_n^2 \omega_n^2)} > 0$$

for some $n \in (2k\pi/R, (2k+1)\pi/R)$ ($k \in \mathbb{N}$). \square

From Lemmas 3.1–3.3, we derive the following results.

Theorem 3.3. Let $\bar{d}_3^*(\gamma)$ and $\bar{d}_3^{**}(\gamma)$ be (3.8) and (3.9), $\bar{d}_{3N}^*(\gamma)$ and $\bar{d}_{3M}^{**}(\gamma)$ be defined as in Lemma 3.1 for $n \in (2k\pi/R, (2k+1)\pi/R)$ ($k \in \mathbb{N}$). Then the following results hold for (1.1) in (γ, d_3) plane.

- (i) n -mode Turing bifurcations occur at $d_3 = \bar{d}_3^*(\gamma)$. Therefore, n -mode nonhomogeneous steady states emerge near E^* .
- (ii) n -mode Hopf bifurcations occur at $d_3 = \bar{d}_3^{**}(\gamma)$. Thus, spatially nonhomogeneous periodic solutions can arise near E^* .
- (iii) For some γ , E^* is locally stable as $\bar{d}_{3N}^*(\gamma) < d_3 < \bar{d}_{3M}^{**}(\gamma)$, and unstable for $d_3 \in (-\infty, \bar{d}_{3N}^*(\gamma)) \cup [\bar{d}_{3M}^{**}(\gamma), +\infty)$.

Similarly, taking R as the bifurcation parameter, we can get the joint influence of the perceptual range and cognitive diffusion by Theorem 3.3 and [30].

Lemma 3.4. If there exists R^* satisfying:

- (i) $A_0(E^*)B_0(E^*) - C_{01}(E^*) = 0$;
- (ii) $\exists \bar{i} \in \mathbb{N}$ satisfies $C_{\bar{i}1}(E^*) = 0$, $A_{\bar{i}}(E^*)B_{\bar{i}}(E^*) - C_{\bar{i}1}(E^*) > 0$. For $i \in \mathbb{N}_0 \setminus \{0, \bar{i}\}$, $C_{i1}(E^*) > 0$, $A_i(E^*)B_i(E^*) - C_{i1}(E^*) > 0$;
- (iii)

$$\left. \frac{d(A_0(E^*)B_0(E^*) - C_{01}(E^*))}{dd_3} \right|_{(R, d_3)=(R^*, \bar{d}_3^{**})} \neq 0; \quad \left. \frac{d(C_{\bar{i}1}(E^*))}{dd_3} \right|_{(R, d_3)=(R^*, \bar{d}_3^{**})} \neq 0,$$

then system (1.1) may exhibit Turing-Hopf bifurcations at E^* as $(R, d_3) = (R^*, \bar{d}_3^{**})$.

Remark 3.1. According to Theorem 3.3, the perception range R significantly influences the dynamics of the three populations. Due to the combined effect of nonlocal perception and the spatial memory diffusion, (1.1) exhibits more complex bifurcation such as Turing–Hopf bifurcation. These results appear richer than those in [17]. Biologically, the emergence of a spatially nonhomogeneous Hopf bifurcation in system (1.1) suggests that the populations may not only develop periodic spatial patterns but also vary across different regions. Furthermore, due to the nonlocal nature of consumer perception, the populations may fail to stabilize at a uniform equilibrium, instead exhibiting uneven spatial distributions. In other words, distinct areas may display different population patterns.

Lemma 3.4 reveals that system (1.1) may exhibit rich dynamics in the vicinity of the bifurcation point (R^*, \bar{d}_3^{**}) . These dynamics include the emergence of spatially inhomogeneous steady states, as well as both spatially homogeneous and inhomogeneous periodic solutions. Consequently, the population distributions may display a variety of spatiotemporal patterns, such as spatially uneven distributions, temporally periodic but spatially uniform patterns, or patterns that are both temporally periodic and spatially heterogeneous.

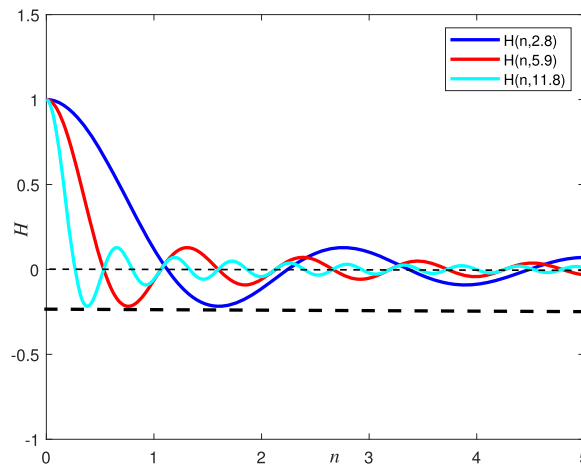


Fig. 10. The curves $H = H(n, R)$. The minimum of $H(n, R) \approx -0.202$.

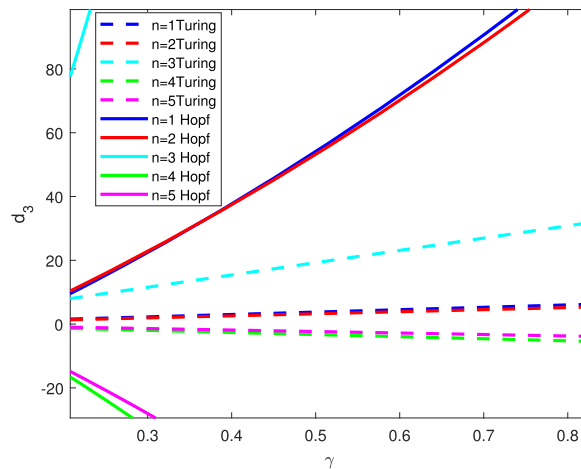


Fig. 11. The bifurcation diagram of (1.1) in (γ, d_3) plane.

In the following, numerical simulations are conducted using the parameters $d_1 = 0.01$, $d_2 = 0.02$, $b = 0.15$, $s = 0.1$, and $\beta = 1$. The resulting population distributions are illustrated accordingly. Fig. 10 shows that the minimum value of $H(n, R)$ remains consistently around -0.202 . For $R = 1$, the Turing and Hopf bifurcation curves are plotted in the (γ, d_3) plane, as shown in Fig. 11. When $m = 1.1$, spatially homogeneous periodic solutions emerge, as depicted in Fig. 12. This suggests that consumers tend to form periodic spatial patterns when encountering abundant resources. While resources are uniformly distributed, consumers display a mixture of dot and stripe patterns. Biologically, frequent interactions between resources and consumers result in a stable distribution of resources and implicit memory effects, whereas consumers exhibit complex, mixed spatial patterns. These phenomena are not observed in system (2.1). Fig. 13 presents additional Turing and Hopf bifurcation curves in the (R, d_3) plane for $\gamma = 0.1$. Notably, the intersection points of these curves correspond to Turing-Hopf bifurcation points.

For $m = 1.1$, $d_3 = 1$, and $R = 1.29$, spatially homogeneous periodic solutions emerge, as shown in Fig. 14. This suggests that, under moderate interaction between resources and consumers, and with a moderate perceptual range, consumers exhibit periodic behavior. Unlike system (2.1), system (1.1) produces spatially homogeneous periodic solutions as a result of nonlocal perception. As the perceptual range of consumers increases, their densities tend to adopt a periodic temporal distribution. Meanwhile, both resources and implicit memory stabilize at their respective maximum levels.

For $d_3 = -1$, Fig. 15 illustrates the emergence of various spatiotemporal patterns. In the absence of perceptual range ($R = 0$), all populations stabilize through local perception. When the perceptual range is small ($R = 1$), the implicit memory develops a square pattern, while the resources and consumers exhibit stripe patterns. At $R = 1$, the domain of the implicit memory contracts, yet the stripe patterns for resources and consumers persist. As the perceptual range increases to $R = 2$, the implicit memory transitions to a spot pattern, while the distributions of resources and consumers evolve into thinner stripe patterns. With further increases in perceptual range, the implicit memory continues to exhibit spot patterns, and the stripe patterns in resource and consumer distributions become increasingly refined.

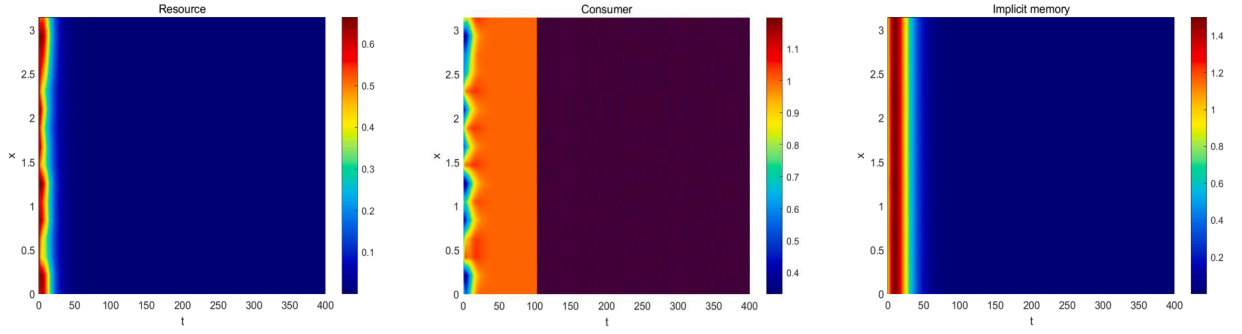


Fig. 12. Patterns near Hopf bifurcation curves for (1.1).

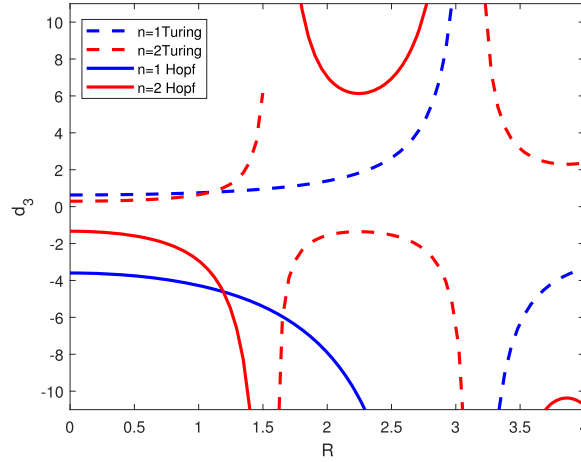


Fig. 13. The bifurcation diagram of (1.1) in (R, d_3) plane.

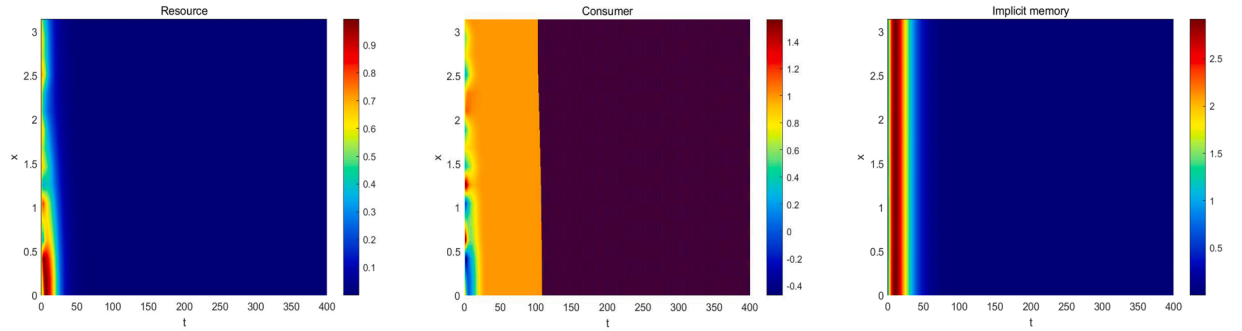


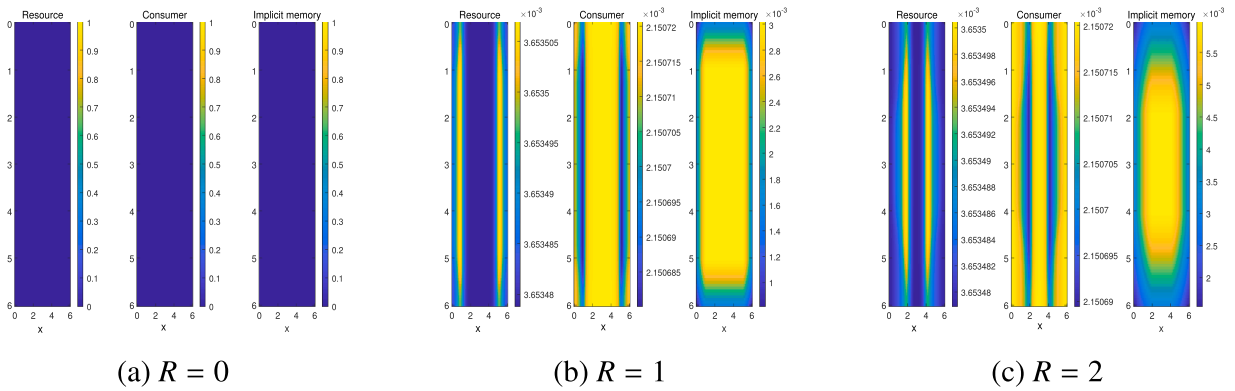
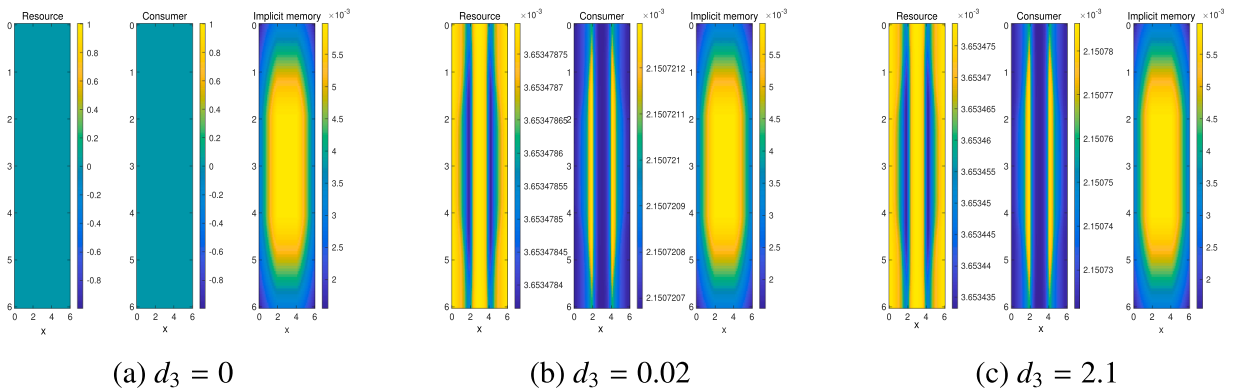
Fig. 14. Patterns near Hopf bifurcation curves for (1.1).

Fixing the perceptual range at $R = 2$, Fig. 16 illustrates various spatiotemporal pattern formation scenarios influenced by cognitive diffusion. In the absence of cognitive diffusion, the resources and consumers remain stable, while the implicit memory continues to exhibit a dot pattern. When consumers spread more rapidly due to cognitive effects, the resources and consumers develop spatially stripe pattern distributions, and the implicit memory adopts a dot-patterned distribution. However, regardless of the rate at which consumers spread in response to cognition, the distributions of all three populations eventually reach a steady state.

From the above results, it is evident that in system (1.1), all three populations transit into distinct patterns, which are not observed in system (2.1).

3.2. Dynamics of (1.2)

In this subsection, we analyze the dynamics of system (1.2). Consider the positive constant equilibrium E_{**} which is locally stable in the corresponding non-spatial system.

Fig. 15. Spatiotemporal patterns for (1.1) with $d_3 = -1$.Fig. 16. Spatiotemporal patterns for (1.1) with $R = 2$.

Linearizing system (1.2) at E_* , we obtain

$$\hat{\mathfrak{L}}_1 \begin{pmatrix} \phi \\ \psi \\ \varphi \end{pmatrix} = \begin{pmatrix} d_1 \Delta \phi + (1 - \beta\alpha - \frac{m\alpha}{(\alpha+1)^2})\phi - \frac{m\alpha}{\alpha+1}\psi \\ d_2 \Delta \psi - d_3 \alpha \Delta \varphi + s\phi + (s-2)\psi \\ \frac{b\alpha\gamma}{\gamma+\xi\alpha}\psi - (\gamma+\xi\alpha)\varphi \end{pmatrix}, \quad (3.14)$$

where α is defined as before. Here, linear operator $\hat{\mathfrak{L}}_1$ is closed in Y with $D(\hat{\mathfrak{L}}_1) = X$. We give results on spectrum of $\hat{\mathfrak{L}}_1$.

Theorem 3.4. Let $\hat{\mathfrak{L}}_1 : X \rightarrow Y$. Its spectrum satisfies

$$\sigma(\hat{\mathfrak{L}}_1) = \sigma_p(\hat{\mathfrak{L}}_1) = \hat{S} \cup \{-\gamma - \xi\alpha\},$$

where

$$\hat{S} = \{\hat{\mu}_{n*}^{(1)}\}_{n=0}^{+\infty} \cup \{\hat{\mu}_{n*}^{(2)}\}_{n=0}^{+\infty} \cup \{\hat{\mu}_{n*}^{(3)}\}_{n=0}^{+\infty}, \quad (3.15)$$

and $\hat{\mu}_{n*}^{(j)}$ ($j = 1, 2, 3$) are roots of the characteristic equation

$$\lambda^3 + \hat{A}_n \lambda^2 + \hat{B}_n \lambda + \hat{C}_{n1} = 0$$

with $\Re(\hat{\mu}_{n*}^{(1)}) < \Re(\hat{\mu}_{n*}^{(2)}) < \Re(\hat{\mu}_{n*}^{(3)})$. Here

$$\begin{aligned} \hat{C}_{n1} &= [d_1 \mu_n - 1 + \beta\alpha + \frac{m\alpha}{(\alpha+1)^2}][d_2 \mu_n - s + 2][\gamma + \xi\alpha] - \frac{b\alpha^2 \gamma d_3 \mu_n}{\gamma + \xi\alpha} [d_1 \mu_n - 1 + \beta\alpha + \frac{m\alpha}{(\alpha+1)^2}] \\ &+ \frac{d_3 b m \alpha^3}{\alpha+1} H(R, n) \mu_n + \frac{[\gamma + \xi\alpha] s m \alpha}{\alpha+1}. \end{aligned}$$

The proof of Theorem 3.4 is similar to Theorem 3.1 and omitted. Thus, we get the following results.

Theorem 3.5. E_* is locally stable in system (1.2) when all the roots of the characteristic equation own negative real parts; otherwise, it is unstable.

By Theorems 3.4–3.5, we derive the steady-state bifurcation condition $\hat{C}_{n1} = 0$, which gives

$$\tilde{d}_3^*(\gamma) = \left\{ \frac{b\alpha^2\gamma\mu_n}{\gamma + \xi\alpha} [d_1\mu_n - 1 + \alpha\beta + \frac{m\alpha}{(\alpha+1)^2}] - \frac{b\alpha^3}{\alpha+1} H(R, n)\mu_n \right\}^{-1} \left\{ [d_1\mu_n - 1 + \beta\alpha + \frac{m\alpha}{(\alpha+1)^2}] [d_2\mu_n - s + 2] [\gamma + \xi\alpha] + \frac{[\gamma + \xi\alpha]s\alpha}{\alpha+1} \right\}. \quad (3.16)$$

Similarly, the condition $\hat{A}_n\hat{B}_n - \hat{C}_{n1} = 0$ yields

$$\tilde{d}_3^{**}(\gamma) = \left\{ \frac{b\alpha^2\gamma\mu_n}{\gamma + \xi\alpha} [d_1\mu_n - 1 + \alpha\beta + \frac{m\alpha}{(\alpha+1)^2}] - \frac{b\alpha^3}{\alpha+1} H(R, n)\mu_n \right\}^{-1} \left\{ [d_1\mu_n - 1 + \beta\alpha + \frac{m\alpha}{(\alpha+1)^2}] [d_2\mu_n - s + 2] [\gamma + \xi\alpha] + \frac{[\gamma + \xi\alpha]s\alpha}{\alpha+1} + \hat{A}_n\hat{B}_n \right\}. \quad (3.17)$$

The following analysis focuses on the properties of the Turing bifurcation curves $d_3 = \tilde{d}_3^*(\gamma)$.

Lemma 3.5. Let $\tilde{d}_3^*(\gamma)$ and $\tilde{d}_3^{**}(\gamma)$ be defined as in (3.16) and (3.17). Then the following results hold for some $n \in (2k\pi/R, (2k+1)\pi/R)$ ($k \in \mathbb{N}$):

- (i) There exist \tilde{n}^* such that for $n \leq \tilde{n}^*$, $\tilde{d}_3^*(\gamma) < 0$, and \tilde{N} with $d_{3\tilde{N}}^*(\gamma) = \max \tilde{d}_3^*(\gamma)$ for $\gamma > 0$; For $n > \tilde{n}^*$, $\tilde{d}_3^*(\gamma) < 0$ when $\gamma \in (0, \tilde{\gamma}_n^*)$, and $\tilde{d}_3^*(\gamma) > 0$ when $\gamma \in (\tilde{\gamma}_n^*, +\infty)$, where $\tilde{\gamma}_n^*$ satisfies $\frac{1}{\tilde{d}_3^*(\tilde{\gamma}_n^*)} = 0$. Moreover, $\tilde{d}_3^*(\gamma)$ is strictly decreasing in n for fixed γ and satisfies

$$\tilde{d}_3^*(\gamma) > \tilde{d}_{3\infty}^*(\gamma) = \frac{d_2[\gamma + \xi\alpha]^2}{b\alpha^2\gamma}, \quad (3.18)$$

where $\tilde{d}_{3\infty}^*(\gamma)$ decreases for $\gamma \in (0, \gamma^*)$ and increases for $\gamma \in (\gamma^*, +\infty)$ with $\gamma^* = \alpha\xi$.

- (ii) There exists \tilde{M} such that $d_{3\tilde{M}}^{**}(\gamma) = \min \tilde{d}_3^{**}(\gamma)$ with fixed $\gamma > 0$, $\tilde{M} \in \mathbb{N}$.

Similar to Lemma 3.4, we can derive the properties of eigenvalues for the characteristic equation.

Lemma 3.6. Let $\tilde{d}_3^*(\gamma)$ and $\tilde{d}_3^{**}(\gamma)$ be defined as in (3.16) and (3.17), and $d_{3\tilde{N}}^*(\gamma)$, $d_{3\tilde{M}}^{**}(\gamma)$ as in Lemma 3.4. Then for $n \in (2k\pi/R, (2k+1)\pi/R)$ ($k \in \mathbb{N}$), the following conclusions hold.

- (i) When $d_{3\tilde{N}}^*(\gamma) < d_3 < \min\{d_{3\tilde{M}}^{**}(\gamma), \tilde{d}_{3\infty}^*(\gamma)\}$, all eigenvalues of the characteristic equation own negative real parts.
- (ii) When $d_3 \geq \min\{d_{3\tilde{M}}^{**}(\gamma), \tilde{d}_{3\infty}^*(\gamma)\}$, the characteristic equation owns a pair of purely imaginary roots at $d_3 = \tilde{d}_3^{**}(\gamma)$.
- (iii) When $d_3 \leq d_{3\tilde{N}}^*(\gamma)$ or $d_3 \geq \min\{d_{3\tilde{M}}^{**}(\gamma), \tilde{d}_{3\infty}^*(\gamma)\}$, the characteristic equation owns a zero root at $d_3 = \tilde{d}_3^*(\gamma)$.

In the following, we verify the transversality condition for Hopf bifurcation in system (1.2) and omit the proof.

Lemma 3.7. The characteristic equation has roots as $\tilde{\lambda} = \tilde{\lambda}(d_3) \pm i\tilde{\omega}(d_3)$ for d_3 near $\tilde{d}_3^{**}(\gamma)$ with $\tilde{\lambda}(\tilde{d}_3^{**}(\gamma)) = 0$ and $\tilde{\lambda}'(\tilde{d}_3^{**}(\gamma)) > 0$ for some $n \in (2k\pi/R, (2k+1)\pi/R)$ ($k \in \mathbb{N}$).

From Lemmas 3.4–3.6, we obtain the stability and bifurcations of the positive steady state of system (1.2).

Theorem 3.6. Let $\tilde{d}_3^*(\gamma)$ and $\tilde{d}_3^{**}(\gamma)$ be defined as in (3.16) and (3.17), $d_{3\tilde{N}}^*(\gamma)$ and $d_{3\tilde{M}}^{**}(\gamma)$ as in Lemma 3.4. Then for (1.2) with some $n \in (2k\pi/R, (2k+1)\pi/R)$ ($k \in \mathbb{N}$),

- (i) n -mode Turing bifurcations occur at $d_3 = d_{3\tilde{N}}^*(\gamma)$ with $\gamma > 0$, producing n -mode nonhomogeneous steady states near E_* ;
- (ii) n -mode Hopf bifurcations occur at $d_3 = d_{3\tilde{M}}^{**}(\gamma)$ for $\gamma > 0$, generating spatially nonhomogeneous periodic solutions near E_* ;
- (iii) for fixed $\gamma \in (0, +\infty)$, E_* is locally stable when $d_{3\tilde{N}}^*(\gamma) < d_3 < \min\{d_{3\tilde{M}}^{**}(\gamma), \tilde{d}_{3\infty}^*(\gamma)\}$; otherwise unstable.

Similarly, taking R as the bifurcation parameter, we can get the joint influence of the perceptual range and cognitive diffusion according to Theorem 3.6 and [30].

Lemma 3.8. If there exists R_* satisfies:

- (i) $\hat{A}_0(E_*)\hat{B}_0(E_*) - \hat{C}_{01}(E_*) = 0$;
- (ii) $\exists \tilde{i} \in \mathbb{N}$ satisfies $\hat{C}_{\tilde{i}1}(E_*) = 0$, $\hat{A}_{\tilde{i}}(E_*)\hat{B}_{\tilde{i}}(E_*) - \hat{C}_{\tilde{i}1}(E_*) > 0$. For $i \in \mathbb{N}_0 \setminus \{0, \tilde{i}\}$, $\hat{C}_{i1}(E_*) > 0$, $\hat{A}_i(E_*)\hat{B}_i(E_*) - \hat{C}_{i1}(E_*) > 0$;
- (iii)

$$\left| \frac{d(\hat{A}_0(E_*)\hat{B}_0(E_*) - \hat{C}_{01}(E_*))}{dd_3} \right|_{(R, d_3)=(R_*, \tilde{d}_3^{**})} \neq 0; \quad \left| \frac{d(\hat{C}_{\tilde{i}1}(E_*))}{dd_3} \right|_{(R, d_3)=(R_*, \tilde{d}_3^{**})} \neq 0,$$

then system (1.2) may exhibit Turing-Hopf bifurcations at E_* as $(R, d_3) = (R_*, \tilde{d}_3^{**})$.

Remark 3.2. Theorem 3.6 indicates that the perceptual range R influences the dynamics of the three populations. Due to the combined effect of nonlocal perception and the spatial memory diffusion, (1.2) exhibits more complex bifurcation such as Turing-Hopf bifurcation. These results appear richer than those in [17]. Lemma 3.8 reveals that system (1.2) can exhibit complex dynamics in the vicinity of (R_*, \tilde{d}_3^{**}) . These dynamics may include spatially inhomogeneous steady states, as well as both spatially homogeneous and inhomogeneous periodic solutions. Consequently, the distributions may display a variety of spatiotemporal patterns, such as spatially uneven steady states, temporally periodic yet spatially uniform distributions, or patterns that are periodic in time and uneven in space.

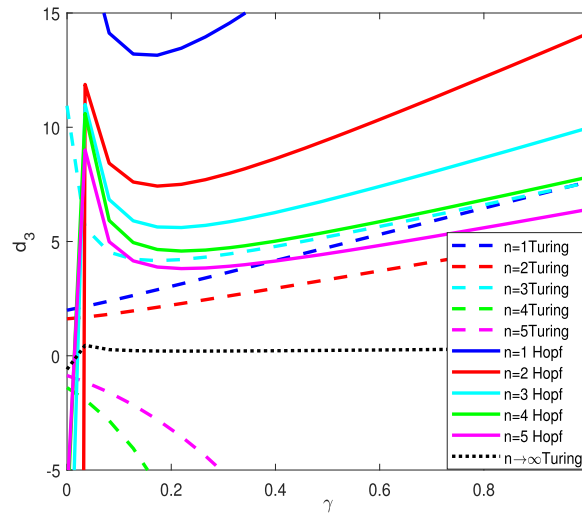


Fig. 17. The bifurcation diagram of (1.2) in (γ, d_3) plane with $R = 1$.

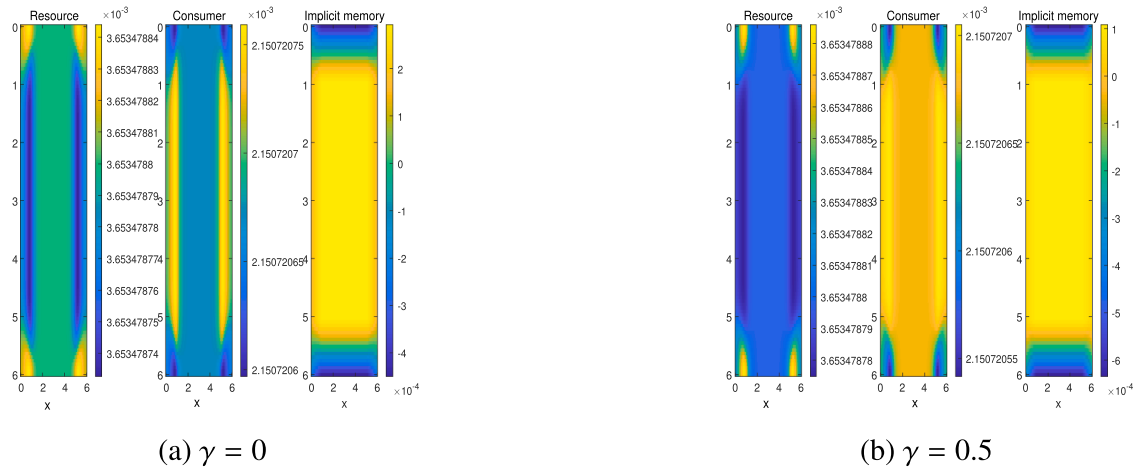
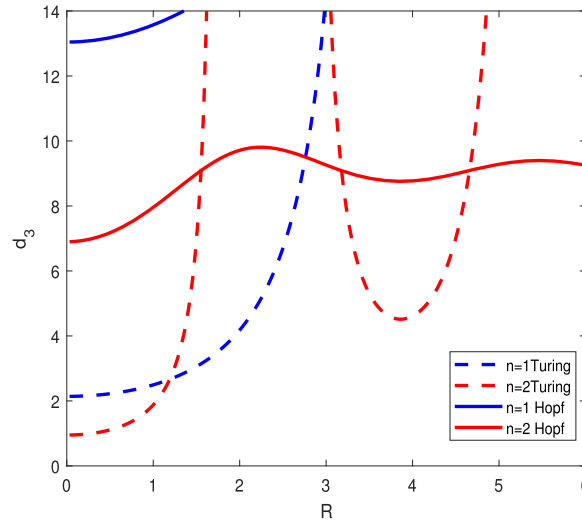
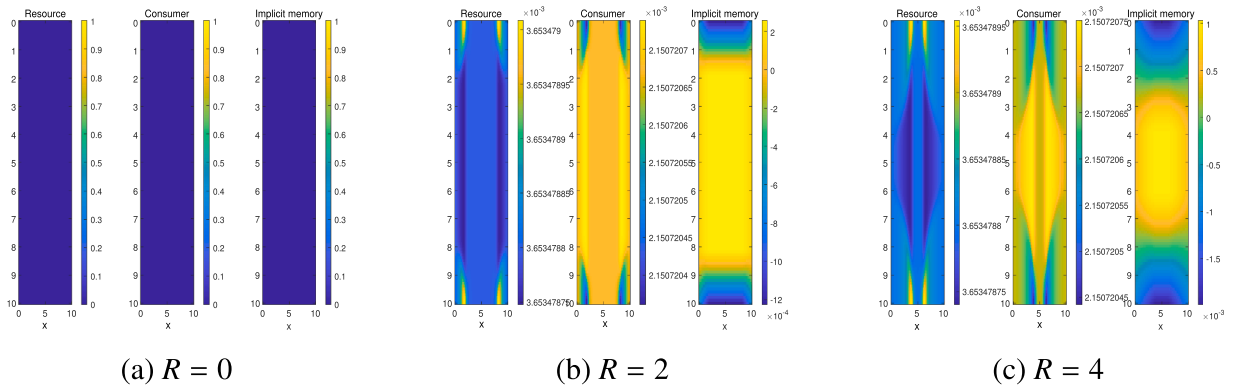
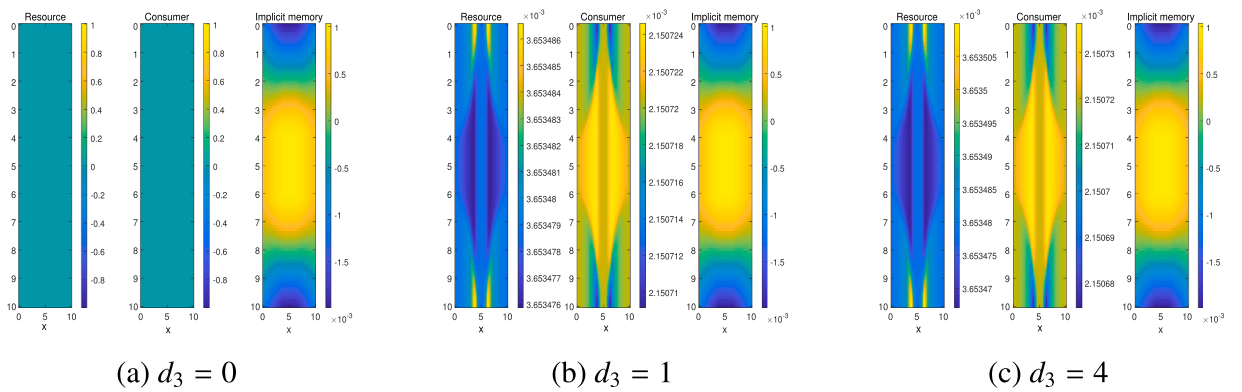


Fig. 18. Spatiotemporal patterns for (1.2) with $d_3 = 0.02$, $R = 1$.

In the following, we present numerical simulations with fixed parameters: $d_1 = 0.01$, $d_2 = 0.02$, $b = 0.15$, $s = 0.1$, $\xi = 0.3$, and $\beta = 1$. The distributions of populations are illustrated. Fig. 17 shows the Turing and Hopf bifurcation curves in the (γ, d_3) plane for $R = 1$. Notably, a limiting Turing bifurcation curve $d_3 = \hat{d}_{3\infty}^*(\gamma)$ appears for infinite modes, which can destabilize system (1.2) when $d_3 > \hat{d}_{3\infty}^*(\gamma)$. For $d_3 = 0.02$ and $R = 1$, spatiotemporal pattern formations are observed, as illustrated in Fig. 18. When $\gamma = 0$, the resources and consumers exhibit hyperbolic patterns, while the implicit memory displays square patterns. As γ increases further, the octagonal patterns of the resources and consumers expand, and the square patterns of the implicit memory grow correspondingly. These results highlight how the memory decay rate γ influences spatial pattern transitions within the ecological system.

Fig. 19 presents the Turing and Hopf bifurcation curves in the (R, d_3) plane for $\gamma = 0.1$, where their intersections correspond to Turing-Hopf bifurcation points. Fig. 20 illustrates the influence of perceptual range R on pattern formation for $d_3 = 0.02$ and $\gamma = 0.1$. When the perceptual range is absent ($R = 0$), all populations remain stable. For small R , bar patterns emerge in the implicit memory, while the resources and consumers exhibit octagonal patterns. As R increases to 4, the implicit memory develops finer bar structures, and the resources and consumers display star-like patterns. These observations suggest that population densities remain stable when consumers possess only local perception. However, with nonlocal perception, the densities of resources and consumers become spatially aggregated at varying scales. Notably, larger perceptual ranges result in weaker aggregation, with lower concentrations of both resources and consumers.

For $R = 4$ and $\gamma = 0.1$, Fig. 21 explores the role of cognitive diffusion. In the absence of cognitive diffusion, the resources and consumers reach a stable state, while the implicit memory exhibits spot patterns. When cognitive diffusion is introduced, the implicit memory retains its spot patterns, but the resources and consumers evolve into a central vertical band that expands toward the four corners, forming an “X” or hourglass shape patterns with spatially varying densities. These patterns reach steady states regardless

Fig. 19. The bifurcation diagram of (1.2) in (R, d_3) plane with $\gamma = 0.1$.Fig. 20. Spatiotemporal patterns for (1.2) with $d_3 = 0.02$, $\gamma = 0.1$.Fig. 21. Spatiotemporal patterns for (1.2) with $R = 4$, $\gamma = 0.1$.

of the speed of cognitive diffusion. This indicates that even though consumers possess nonlocal perceptual capabilities, the system remains stable as long as the perception itself is not diffused. In this scenario, consumers' perceptual range remains fixed and effective. However, once cognitive diffusion is activated, regardless of its intensity, it drives the aggregation of resources and consumers.

These results highlight two key findings: the perceptual range R governs the transition of spatial patterns from steady states to star patterns via intermediate octagonal structures; and system (1.2) exhibits richer pattern diversity than systems (1.1)/(2.2), primarily due to the effects of nonlocal perception.

4. Discussion

In light of the role of cognition in animal movement, increasing attention has been devoted to the study of spatial memory. Numerous studies have explored this topic [7,9,10,12–16,23]. In particular, [6] introduced the concept of implicit memory using a learning-based approach, distinguishing it from the more commonly studied explicit memory. While many existing works focus on the influence of explicit memory, investigations into implicit memory remain limited. More recently, [17] examined two consumer-resource models incorporating implicit memory based on local perception. Building upon this, we focus on two diffusive resource-consumer systems that integrate both implicit memory and nonlocal perception. Compared to [17], our model adopts a top-hat function as the kernel for nonlocal perception, which is more biologically realistic. The objective should be to investigate effects of cognitive diffusion and perceptual range. To this end, we analyze the system dynamics both in the absence and presence of nonlocality.

On one hand, since systems (1.1)–(1.2) and (2.1)–(2.2) consist of PDE-ODE couplings, their analysis is more challenging than that of classical reaction-diffusion systems. On the other hand, we treat cognitive diffusion and perceptual range as bifurcation parameters to investigate the conditions under which bifurcations occur. Our theoretical and numerical results show that both Turing and Hopf bifurcations can arise with or without nonlocal perception. In the absence of nonlocality, system (2.2) displays especially rich dynamics: the combined effects of cognitive diffusion and memory decay rate can generate four-mode or five-mode periodic patterns, as well as quasi-periodic structures. Biologically, this implies the existence of complex population distributions characterized by nonhomogeneous periodicity in multiple spatial modes.

Furthermore, when nonlocality is included, the systems may undergo Turing-Hopf bifurcations, leading to an even wider array of spatial patterns. These include stripes, spots, and hybrid structures resulting from the interplay between cognitive diffusion and perceptual range. Such phenomena are novel outcomes of nonlocal perception and stand in stark contrast to the findings of [17], underscoring the substantial influence of implicit memory and cognitive diffusion on animal movement.

Our work offers new insights into animal movement by demonstrating that systems (1.1)–(1.2), which incorporate implicit memory and nonlocal perception, produce much richer pattern dynamics than models limited to local perception. From a biological perspective, this reflects realistic ecological constraints in which animals navigate bounded habitats while maintaining broad perceptual awareness, resulting in intricate spatial distributions. The framework of nonlocal perception thus provides a more accurate representation of animal movement and resource-consumer interactions. However, this study focuses only on dynamics near constant steady states in 1D domain. The dynamics associated with non-constant steady states remain unexplored in multi-dimensional domains. In future work, we aim to address this gap, and extend the current approach to include advanced nonlocal perception models incorporating time delays and multi-scale habitat structures in multi-dimensional domains or computing Turing-Hopf normal forms or global attractors for future work.

CRedit authorship contribution statement

Luhong Ye: Writing – review & editing, Writing – original draft, Visualization, Methodology, Funding acquisition, Formal analysis;
Hao Wang: Writing – review & editing, Supervision, Methodology, Investigation, Conceptualization.

Data availability

No data was used for the research described in the article.

Declaration of competing interest

The authors declare that they have no known competing financial interests or personal relationships that could have appeared to influence the work reported in this paper.

Acknowledgement

We express our sincere gratitude to the handling editor and two anonymous reviewers for their careful reading and valuable suggestions, which significantly improved the quality of our paper. Luhong Ye's research was partially supported by the faculty education project of [Anqing Normal University \(ASRSC023\)](#). Hao Wang's research was partially supported by the Natural Sciences and Engineering Research Council of Canada ([Individual Discovery Grant \(RGPIN-2020-03911\)](#)) and [Discovery Accelerator Supplement Award \(RGPAS-2020-00090\)](#) and the [Canada Research Chairs program \(Tier 1 Canada Research Chair Award\)](#).

References

- [1] Fagan WF, Lewis MA, Auger-Méthé M, Avgar T, Benhamou S, Breed G, et al. Spatial memory and animal movement. *Ecol Lett* 2013;16(10):1316–29.
- [2] Fagan WF, Gurarie E, Bewick S, Howard A, Cantrell RS, Cosner C. Perceptual ranges, information gathering, and foraging success in dynamic landscapes. *Am Nat* 2017;189(5):474–89.
- [3] Fagan WF. Migrating whales depend on memory to exploit reliable resources. *Proc National Acad Sci* 2019;116(12):5217–19.
- [4] Abrahms B, Hazen EL, Aikens EO, Savoca MS, Goldbogen JA, Bograd SJ, et al. Memory and resource tracking drive blue whale migrations. *Proc National Acad Sci* 2019;116(12):5582–7.
- [5] Potts JR, Lewis MA. Spatial memory and taxis-driven pattern formation in model ecosystems. *Bull Math Biol* 2019;81:2725–47.

- [6] Wang H, Salmani Y. Open problems in PDE models for knowledge-based animal movement via nonlocal perception and cognitive mapping. *J Math Biol* 2023;86(5):71.
- [7] Wang C, Yuan S, Wang H. Spatiotemporal patterns of a diffusive prey-predator model with spatial memory and pregnancy period in an intimidatory environment. *J Math Biol* 2022;84(3):12.
- [8] Shi J, Wang C, Wang H, Yan X. Diffusive spatial movement with memory. *J Dynam Differen Equat* 2020;32:979–1002.
- [9] An Q, Wang C, Wang H. Analysis of a spatial memory model with nonlocal maturation delay and hostile boundary condition. *Discr Contin Dynam Syst* 2020;40(10).
- [10] Shi J, Wang C, Wang H. Diffusive spatial movement with memory and maturation delays. *Nonlinearity* 2019;32(9):3188.
- [11] Shi Q, Shi J, Wang H. Spatial movement with distributed memory. *J Math Biol* 2021;82(4):33.
- [12] Song Y, Shi J, Wang H. Spatiotemporal dynamics of a diffusive consumer-resource model with explicit spatial memory. *Stud Appl Math* 2022;148(1):373–95.
- [13] Song Y, Wu S, Wang H. Spatiotemporal dynamics in the single population model with memory-based diffusion and nonlocal effect. *J Differ Equ* 2019;267(11):6316–51.
- [14] Song Y, Wu S, Wang H. Memory-based movement with spatiotemporal distributed delays in diffusion and reaction. *Appl Math Comput* 2021;404:126254.
- [15] Ye L, Zhao H, Wu D. Dynamical analysis of a spatial memory prey–predator system with gestation delay and strong allee effect. *Zeitschrift für angewandte Mathematik und Physik* 2024;75(1):29.
- [16] Li S, Yuan S, Jin Z, Wang H. Bifurcation analysis in a diffusive predator-prey model with spatial memory of prey, allee effect and maturation delay of predator. *J Differ Equ* 2023;357:32–63.
- [17] Shi Q, Song Y, Wang H. Local perception and learning mechanisms in resource-consumer dynamics. *SIAM J Appl Math* 2024;84(3):988–1010.
- [18] Furter J, Grinfeld M. Local vs. non-local interactions in population dynamics. *J Math Biol* 1989;27:65–80.
- [19] Bo X, Chu C, Liu W, Lv G, Zhang X. Bifurcation and stability analysis of cognitive populations in toxic environments. *Commun Nonlinear Sci Numer Simul* 2025;108674.
- [20] Wang K, Wang H, Zhao H. On the role of advection in a spatial epidemic model with general boundary conditions. *J Differ Equ* 2024a;386:45–79.
- [21] Djilali S. Pattern formation of a diffusive predator-prey model with herd behavior and nonlocal prey competition. *Math Methods Appl Sci* 2020;43(5):2233–50.
- [22] Geng D, Jiang W, Lou Y, Wang H. Spatiotemporal patterns in a diffusive predator–prey system with nonlocal intraspecific prey competition. *Stud Appl Math* 2022;148(1):396–432.
- [23] Liu Y, Duan D, Niu B. Spatiotemporal dynamics in a diffusive predator–prey model with group defense and nonlocal competition. *Appl Math Lett* 2020;103:106175.
- [24] Segal BL, Volpert VA, Bayliss A. Pattern formation in a model of competing populations with nonlocal interactions. *Physica D* 2013;253:12–22.
- [25] Pal S, Ghorai S, Banerjee M. Analysis of a prey–predator model with non-local interaction in the prey population. *Bull Math Biol* 2018;80:906–25.
- [26] Ding X, Song Y. Stability and bifurcation analysis for a general nonlocal predator–prey system with top-hat kernel function. *Nonlinear Dyn* 2024;112(11):9617–37.
- [27] Xue S, Song Y, Wang H. Spatio-temporal dynamics in a reaction-diffusion equation with nonlocal spatial memory. *SIAM J Appl Dyn Syst* 2024;23(1):641–67.
- [28] Chen S, Shi J, Chen GZ. Spatial pattern formation in activator-inhibitor models with nonlocal dispersal. *Discr. Contin. Dyn. Syst.-Series B* 2021;26(4).
- [29] Van Neerven J. Functional analysis; vol. 201. Cambridge University Press; 2022.
- [30] Wang J, Zhao H, Wang H. The role of natural recovery category in malaria dynamics under saturated treatment. *J Math Biol* 2024b;88(3):33.